



# High-frequency sequence stratigraphy of Pennsylvanian-Lower Permian carbonate successions of the Robledo Mountains, New Mexico and the Carnic Alps, Austria: a record of the acme and demise of the late Palaeozoic ice age

Daniel Calvo González<sup>1</sup> · Benoit Beauchamp<sup>1</sup> · Charles M. Henderson<sup>1</sup>

Received: 23 August 2022 / Accepted: 22 November 2022 / Published online: 5 December 2022  
© Springer-Verlag GmbH Germany, part of Springer Nature 2022

## Abstract

The cyclic to non-cyclic Pennsylvanian-Lower Permian successions of the Robledo Mountains, New Mexico and the Carnic Alps, south Austria, record the acme and demise of the late Palaeozoic ice age (LPIA). Microfacies analyses of cyclic strata of the Pennsylvanian-Asselian Horquilla, Shalem Colony (New Mexico), and Schulterkofel (Carnic Alps) formations record glacioeustatic sea-level fluctuations of an amplitude on the order of 100 m. These fluctuations were the result of Milankovitch-driven eustatic sea-level shifts associated with the waxing and waning of ice sheets during the peak of the main phase of the LPIA. Microfacies analyses of the overlying upper Asselian cyclothems of the Community Pit, Robledo Mountains (New Mexico) and Zweikofel (Carnic Alps) formations record relatively moderate sea-level variations on the order of a few tens of metres (~30–40 m). This comparatively minor sea-level amplitude may be linked to the demise of ice sheets during the final stages of the LPIA and the limited input that shrinking ice sheets had on global sea-level fluctuations prior to their final collapse at the Asselian-Sakmarian boundary. The uppermost part of the Robledo Mountains and the Apache Dam (New Mexico) and Zottachkopf (Carnic Alps) formations are Sakmarian. These strata are interpreted as non-cyclic and represent sedimentation following the end of the LPIA.

**Keywords** LPIA · Cyclothem · Pennsylvanian · Permian · Carbonates

## Introduction

The largest glaciation event of the Phanerozoic occurred during the late Palaeozoic: the so-called late Palaeozoic ice age (LPIA) (Eyles 1993; Fielding et al. 2008; Rygel et al. 2008; Lopez-Gamundi and Buatois 2010; Montañez and Poulsen 2013). The LPIA was a multi-phase ice age characterized by alternating glacial (C1, C2, C3 and C4 in the Carboniferous; P1, P2, P3 and P4 in the Permian) and interglacial intervals (Isbell et al. 2003, 2012; Fielding et al. 2008; Gulbranson et al. 2010; Limarino et al. 2014; Vesely et al. 2015; Fallgatter and Paim 2017). The oldest evidence of late Palaeozoic glaciation is recorded in latest Famennian-Viséan glacial deposits across several South American basins (Caputo

et al. 2008). In addition, a global  $\delta^{13}\text{C}$  and  $\delta^{18}\text{O}$  positive anomaly in mid-Tournaisian brachiopod shells and conodont apatite has been interpreted as indirect evidence for organic carbon burial and buildup of glacial ice, respectively (Mii et al. 1999; Saltzman et al. 2000; Buggisch and Joachimski 2006). The demise of the LPIA, normally assumed to have occurred during the Guadalupian, is interpreted from glaciogenic deposits in eastern Australia and New Zealand (Fielding et al. 2008; Mory et al. 2008; Waterhouse and Shi 2010). Various forcing mechanisms have been proposed to explain the onset of glaciation as follows: (i) continental migration of Gondwana; (ii) closure of the Rheic Ocean; (iii) development of topography that facilitated the nucleation of glaciers, and (iv) reduction in atmospheric  $\text{CO}_2$  and surging rates of silicate weathering (Montañez and Poulsen 2013).

Carboniferous and Lower Permian sequences globally are characterized by cyclic deposits, known as parasequences or cyclothems, comprising transgressive–regressive (T-R) marine and non-marine facies (Heckel 1994). These

✉ Daniel Calvo González  
dcalvogo@ucalgary.ca

<sup>1</sup> Department of Geoscience, University of Calgary, 2500 University Dr. NW, Calgary, AB T2N 1N4, Canada

vertically stacked T-R successions were first defined in the Pennsylvanian carbonate and phosphatic black shale successions of eastern Kansas and interpreted to represent fluctuations of base level (Heckel 1977). Currently, these cyclic deposits are interpreted to represent glacioeustatic fluctuations due to the waxing and waning of ice sheets during the LPIA (Dvorjanin et al. 1996; Collins et al. 2006; Stemmerik 2008; Chesnel et al. 2016; Fang et al. 2018). As an example, Serpukhovian–Bashkirian cyclic successions have been reported in the North Greenland-Svalbard-Barents Sea, the Valdorria platform in northern Spain, the Kashagan platform in Kazakhstan, South China, and in the Donets Basin in Ukraine (Dvorjanin et al. 1996; Golonka and Ford 2000; Collins et al. 2006; Chesnel et al. 2016; Fang et al. 2018). Peak glaciation in the Gzhelian-Asselian was accompanied by widespread cyclic deposition in Laurussia that also had an imprint in the geological record (Rygel et al. 2008). Gzhelian-Asselian cyclic sequences have been observed globally across mid-west and south-west USA, western and Arctic Canada, Greenland, Europe, China, India, Southeast Asia, and South America. The interpreted eustatic amplitude recorded by these cyclic deposits varies considerably between authors, ranging between 20 and 155 m (Klein 1994; Joachimski et al. 2006). Although Carboniferous and Lower Permian successions are commonly interpreted as cyclic in response to glacioeustatic sea-level fluctuations, a different school of thought interprets the facies arrangement of these successions to be driven by autogenic processes, rather than by glacioeustasy (Manifold et al. 2020, 2021).

In this paper, detailed microfacies analyses of Lower Permian carbonate-dominated successions from the Robledo Mountains, New Mexico and the Carnic Alps, Austria, are used to estimate variations in the amplitude of sea-level fluctuations during the peak and subsequent demise of the earliest Permian glacial interval. The relative abundances in thin section of environmentally sensitive biotic and abiotic grains, lime mud, and cement along with field observations form the basis for the interpreted estimations in the amplitude of sea-level change. Published small foraminifer, fusulinid and conodont taxa as well as updated and newly collected conodont data are utilized to date the timing of a major shift in the amplitude of sea-level fluctuations during the Early Permian.

## Methods

A total of 336 rock samples were collected in the Branson Canyon and Flood sections in the Robledo Mountains (New Mexico) and in the Garnitzenbach and Zottachkopf sections in the Carnic Alps (Austria) (Fig. 1). Lithosamples from the studied sections were categorized into microfacies based on their texture, grain assemblage, relative proportions of

clastic and carbonate material, and grain-size in thin-section following the Dunham (1962) classification scheme. Additional field observations and photographs complemented microfacies descriptions. Several conodont samples ranging between 4 and 6 kgs in weight were collected at prospective limestone beds in the Community Pit, Robledo Mountains and Apache Dam formations (New Mexico). Standard conodont sample processing techniques were used including dissolution of the carbonate in a 10% acetic acid solution followed by sieving, bleaching of the residue and heavy liquid separation (2.85 specific gravity) of the dry residue. Conodont elements were hand-picked under a binocular microscope and photographed using a scanning electron microscope.

## Microfacies and cyclicity

The studied formations in the Robledo Mountains (New Mexico) include the upper part of the Community Pit, Robledo Mountains and lowermost part of the Apache Dam formations; the studied formations in the Carnic Alps (Austria) include the uppermost part of the Grenzland, Zweikofel, Zottachkopf and lowermost part of the Trogkofel formations (Fig. 2). Eleven microfacies were identified in the Community Pit, Robledo Mountains and Apache Dam formations (Table 1; Figs. 3, 4, 5, 6, 7, 8): MF<sub>RM</sub>1 and MF<sub>RM</sub>2 are interpreted as supratidal to semi-restricted subtidal; MF<sub>RM</sub>3 to MF<sub>RM</sub>6 are considered inner-ramp deposits formed below fair-weather wave base (FWWB) and above the thermocline under low- to high-energy conditions, and MF<sub>RM</sub>7 to MF<sub>RM</sub>11 represent a deeper-water, mid-ramp setting located between FWWB and storm-weather wave base (SWWB), above and below the thermocline. The Zweikofel, Zottachkopf and Trogkofel formations were categorized into 13 microfacies (Table 2; Figs. 9, 10, 11, 12, 13, 14): MF<sub>CA</sub>1 to MF<sub>CA</sub>7 are interpreted as inner-ramp deposits ranging from a high-energy, clastic shoreface environment and an open-marine carbonate depositional setting at and below FWWB under moderate energy conditions, and MF<sub>CA</sub>8 to MF<sub>CA</sub>13 are considered as deeper-water, mid-ramp deposits formed at and below FWWB, and above and below the thermocline in an open-marine environment under normal salinity conditions. Microfacies associations and microfacies trends were used in tandem with field photographic observations to recognise low- and high-frequency sequences in the studied successions and to infer the amplitude of eustatic fluctuations within high-frequency sequences. Conodont and fusulinid biostratigraphic data were applied to interregional correlations in order to date the transition between cyclic to non-cyclic deposits at both measured sections. The end of high-frequency cyclicity is assumed to mark the end of the main phase (P1) of the late Paleozoic ice age (LPIA).

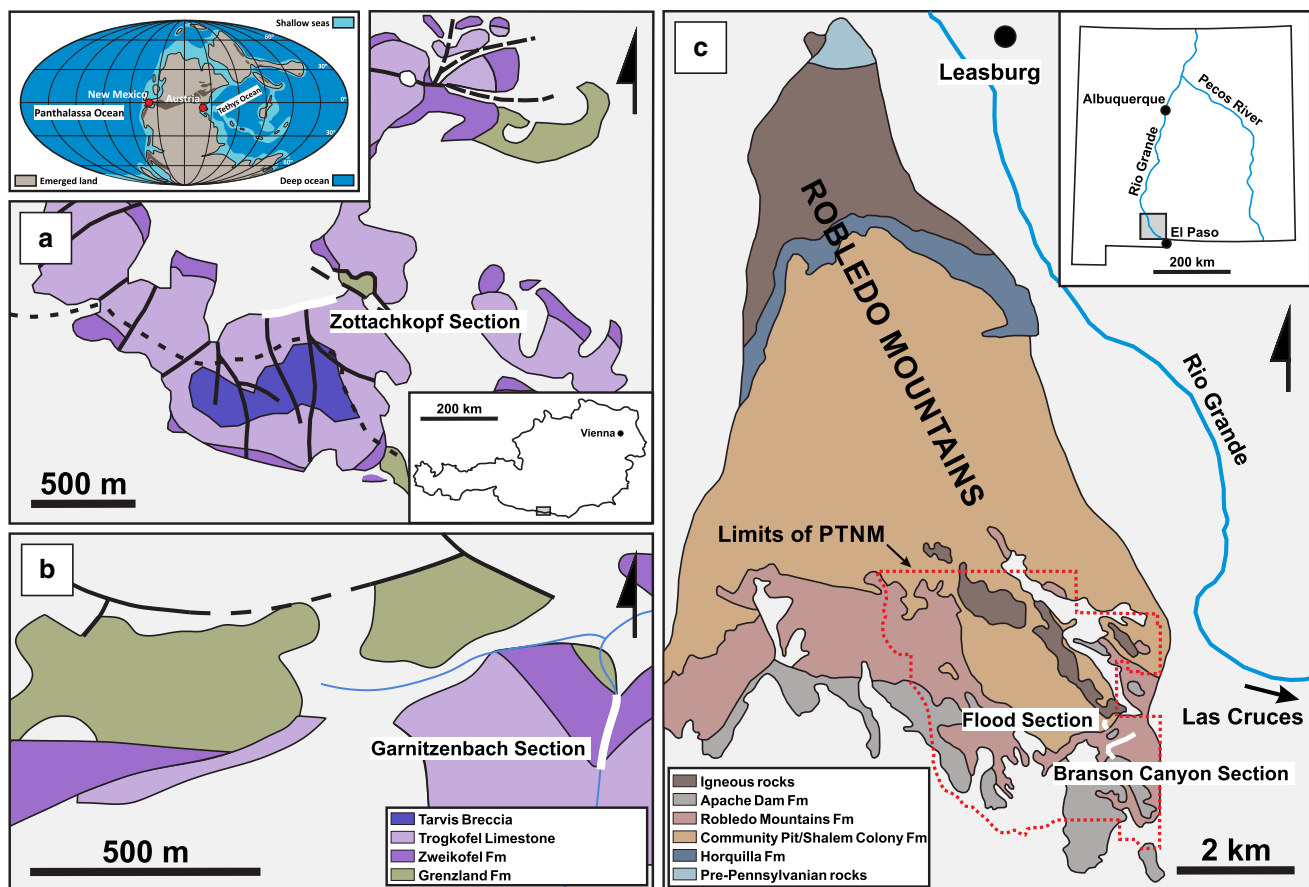


**Fig. 1** a Geological map showing location of the Zottachkopf section along the northern wall of Trogkofel massif in the Carnic Alps; **b** Geological map showing location of the Garnitzenbach section along

Garnitzenklamm gorge, located approximately 1 km east of Trogkofel massif; **c** Geological map showing location of the Branson Canyon and Flood sections in the Robledo Mountains

Low- and high-frequency transgressive–regressive (T-R) sequences were observed in the two study areas. These sequences are composed of a basal deepening-upward transgressive systems tract (TST) followed by a shallowing-upward regressive systems tract (RST). The TST and RST are separated by a maximum flooding surface (MFS). Low-frequency sequences in the studied successions may encompass one entire formation or straddle across two. The time represented by each low-frequency sequence is on the order of a few million years based on conodont and fusulinid biostratigraphy and the current Geologic Time Scale (Henderson and Shen 2020). The boundaries between low-frequency sequences may be conformable or erosional and typically separate two sedimentary successions that contain distinct microfacies suites. High-frequency sequences, also known as cyclothems or parasequences, represent a time span of approximately 400 Kyr and are found nested within low-frequency sequences. The boundaries between high-frequency sequences are concordant contacts that may display evidence of subaerial exposure. Microfacies analysis as well as field observations of the lithology, macrofossils,

sedimentary structures and stratigraphic surfaces was combined to identify low- and high-frequency sequences in the studied successions. Low-frequency sequences were identified in the upper part of the Community Pit, Robledo Mountains, lower part of the Apache Dam, Zweikofel and Zottachkopf formations. High-frequency sequences were observed in the upper part of the Community Pit, Robledo Mountains and Zweikofel formations.

The terms heterozoan and photozoan associations are used throughout this paper. The term heterozoan association, coined by James (1997), refers to the modern assemblage of grains comprising coralline algae and heterotrophic benthic invertebrates that are typically found in modern cool to temperate environments colder than 20 °C or under higher nutrient concentrations (mesotrophic). In modern oceans, heterozoan associations are found in mid- to high-latitudes (> 30° N and > 30° S) or in tropical latitudes below the thermocline or under the right oceanographic conditions, such as in areas affected by cold surficial currents (Logan et al. 1969; Simone and Carannante 1988; Hallock et al. 1988; Carannante et al. 1988; James

		Carnic Alps, Austria		Robledo Mountains, New Mexico	
		Krainer et al., 2019	This study	Lucas et al., 2015	This study
Cisuralian	Kungurian				
		Goggau			
		Trogkofel	Trogkofel		
		Zottachkopf		Apache Dam	
	Zweikofel	Robledo Mountains			
	Artinskian				
	Sakmarian	Grenzland	Zottachkopf	Community Pit	Apache Dam
			Zweikofel		Robledo Mountains
Asselian	Grenzland	Zweikofel	Shalem Colony	Community Pit	
		Grenzland		Shalem Colony	
Pennsylvanian	Gzhelian	Schulterkofel	Horquilla	Horquilla	
	Kasimovian	Auernig Group			Auernig Group

Fig. 2 Current age interpretation of the studied formations based on foraminiferal and conodont biostratigraphy

1997). Similarly, a late Palaeozoic heterozoan association is composed of abundant bryozoans, echinoderms and brachiopods, and rare red algae, bivalves, solitary rugose corals and *Tubiphytes* (Beauchamp and Desrochers 1997).

The term photozoan association, also defined by James (1997), refers to the modern assemblage of grains composed of the aforementioned heterozoan components, in addition to green calcareous algae, corals, invertebrates with a symbiotic relationship with photosynthetic organisms, inozoan and sphinctozoan sponges, ooids, oncoids and peloids; this sediment is found in modern warm-water settings above 20 °C under euphotic and oligotrophic conditions (Beauchamp and Desrochers 1997). In modern oceans, photozoan associations occur in tropical latitudes (between 30° N and 30° S) above the thermocline. A late Palaeozoic photozoan association is composed of abundant calcareous green algae (e.g., dasyclad, phylloid, etc.), calcareous red algae (e.g., *Archaeolithophyllum*), calcareous sponges, colonial rugose corals, oncoids, ooids, and grains from the heterozoan association (Beauchamp and Desrochers 1997).

## Geological setting

### Robledo Mountains

The Branson Canyon and Flood sections are located near the eastern margin of the Prehistoric Trackways National Monument (PTNM), a 5280-acre area of protected land in the southeastern point of the Robledo Mountains approximately 13 km northwest of Las Cruces, southern New Mexico (Figs. 1, 15a, b). These sections comprise bedded limestone, sandstone, siltstone and minor shale of the upper part of the Community Pit, Robledo Mountains and lower part of the Apache Dam formations (Fig. 2). The Robledo Mountains are one of many isolated fault block mountain ranges located either side of the Rio Grande rift system within the Basin and Range Province (Lucas et al. 2015). The Rio Grande rift system is one of many north–south trending extensional basins formed by continuing crustal extension since the Miocene. It extends from northern Mexico to central Colorado and comprises

**Table 1** Description of the eleven microfacies observed in the Community Pit, Robledo Mountains and Apache Dam formations in the Robledo Mountains, New Mexico

Microfacies name	Allochem assemblage	Distribution	Depositional environment
MF <sub>RM1</sub> Siltstone to fine sandstone	Unfossiliferous (Fig. 3a–d)	Present in all red beds in the Robledo Mountains Formation	Supratidal. Possibly a coastal floodplain
MF <sub>RM2</sub> Unfossiliferous mudstone	MF <sub>RM2A</sub> – Laminated m.: Common peloids. Rare ostracods and gastropods (Fig. 3e–f) MF <sub>RM2B</sub> – Nodular m.: Peloids and sponge spicules (Fig. 3g–h)	Found in the Community Pit formation	Intertidal to subtidal
MF <sub>RM3</sub> Spiculitic wackestone-packstone	Abundant siliceous sponge spicules and peloids. Common-rare small and encrusting foraminifers, ostracods and bivalves (Fig. 4a–d)	Common in the Community Pit Formation and absent in the Robledo Mountains formation	Inner ramp. Low energy setting with normal marine salinity
MF <sub>RM4</sub> Mollusc and ostracod wackestone-packstone	MF4A – Ostracod and peloid w-p.: Abundant-common ostracods and peloids. Common-rare apterrinellids, microconchids, small foraminifers and bivalves (Fig. 4e–f) MF4B – Bivalve, ostracod and microconchid p.: Abundant-common bivalves, ostracods and microconchids. Rare apterrinellids, gastropods, peloids and nodosariids (Fig. 4g–h)	Common in the Community Pit Formation and in the Robledo Mountains Formation. Single occurrence at the base of the Apache Dam formation	Inner ramp. Below FWWB and above the thermocline. Low energy setting, possibly a lagoon
MF <sub>RM5</sub> Encrusting foraminifer packstone	Abundant apterrinellids and peloids. Common-rare ostracod, bivalves, gastropods, tubertinids and small foraminifers (Fig. 5a–d)	Found in the Robledo Mountains formation	Inner ramp. Shallow water above the thermocline and below FWWB
MF <sub>RM6</sub> Ooid packstone-grainstone	Abundant-common ooids, peloids, ostracods and globivalvulinitids. Common-rare bivalves, calcareous algae, calcareous sponges, small foraminifers and encrusting foraminifers (Fig. 5e–h)	Community Pit formation	Inner ramp. Very shallow water above the thermocline and FWWB
MF <sub>RM7</sub> Algal wackestone-packstone-rudstone	MF7A – Phylloid algal w-p.: Abundant-common phylloid algal and peloids. Common-rare dasyclad algae, echinoderms, globivalvulinitids, ostracods, gastropods, fusulinids and apterrinellids. Rare small foraminifers, bryozoans, siliceous monoaxon spicules, <i>Girvanella</i> and oncoids (Fig. 6a–d) MF7B – Phylloid and epimastoporoid algal p-r.: Abundant-common dasyclad algae and phylloid algae, encrusting foraminifers, small foraminifers and ostracods (Fig. 6e–h)	Upper half of the Robledo Mountains Formation and throughout the Apache Dam formation	Mid ramp. Shallow water, above thermocline and below FWWB

Table 1 (continued)

Microfacies name	Allochem assemblage	Distribution	Depositional environment
MF <sub>RM8</sub> Oncoïd and algal packstone	Abundant-common oncoïds, dasyclad algae, fusulinids, echinoderms and apterinnellids. Common-rare peloids, small foraminifers, epimastoporoid algae, ostracods, gastropods and bivalves (Fig. 7 a–d)	One occurrence at 144.7 m in the Apache Dam formation at Branson Canyon	Mid ramp. Open marine, below FWWB and above SWWB. Above thermocline
MF <sub>RM9</sub> Algal, echinoderm and small foraminifer packstone	Abundant-common echinoderms, fusulinids, peloids and small foraminifers. Common-rare phylloid algae, encrusting foraminifers, ostracods, bivalves and gastropods (Fig. 7 e–h)	Present in the Robledo Mountains Formation and in the Apache Dam formation	Mid ramp. Open marine, below FWWB and above SWWB. Above thermocline
MF <sub>RM10</sub> Echinoderm, peloid and small foraminifer packstone	Abundant-common echinoderms, globulivulnids, peloids and ostracods. Common-rare encrusting foraminifers, brachiopods, nodosariids and gastropods (Fig. 8 a–d)	Upper Robledo Mountains Formation and upper Apache Dam formation	Mid ramp. Open marine, below FWWB and above SWWB. Below thermocline
MF <sub>RM11</sub> Laminated heterozoan packstone	Abundant echinoderms. Common-rare brachiopods, bryozoans, and ostracods, tuberetinids, and small foraminifers. Rare tuberetinids, globulivulnids, <i>Pseudoagathamina</i> , lastodiscids and nodosariids (Fig. 8 e–h)	Robledo Mountains Formation and Apache Dam formation	Mid ramp. Open marine. Below FWWB and above SWWB. Below thermocline

multiple smaller basins filled by syn-rift alluvial deposits of the Santa Fe Group and mafic volcanics (Lucas et al. 2015).

The oldest strata in the Robledo Mountains outcrop to the north and include Ordovician and Mississippian rocks with an approximate maximum thickness of 300 m (Lucas et al. 2015). Overlying these strata, the Pennsylvanian to lowermost Permian Horquilla Formation outcrops on the northern and western flanks of the Robledo Mountains. The Horquilla Formation reaches a maximum thickness of 300 m and is composed of alternating limestone and shale couplets interpreted as cyclothems (Krainer et al. 2015). The overlying Lower Permian strata, formally upgraded from Hueco Formation to Hueco Group by Lucas et al. (1998), are composed of the Shalem Colony, Community Pit, Robledo Mountains and Apache Dam formations. In the Robledo Mountains, the Shalem Colony Formation conformably overlies the Horquilla Formation. The Shalem Colony ranges between 106 and 127 m in thickness and is composed of bedded limestone and shale interbeds (Lucas et al. 2015). This formation is also interpreted to be composed of cyclothems. The overlying Community Pit Formation was measured at the Flood section (Figs. 1, 15a). At Flood, the upper 103.9 m of the formation is composed of bedded limestone and shale and overlies a Quaternary rhyolitic sill. The lower part of the formation reaches 52.8 m in the Monument North section where it is overlain by the same Quaternary sill (Lucas et al. 2015). Across the Robledo and Doña Ana mountains the thickness of the Community Pit Formation varies between 93 and 177 m (Lucas et al. 2015). The overlying Robledo Mountain Formation was measured at the Branson Canyon section (Figs. 1, 15b). At this locality, a complete section of the formation reaches a thickness of 114.8 m and is composed of bedded limestone, sandstone, siltstone and shale (Fig. 16). Covered intervals are common within the upper third of the formation. The lower part of the Apache Dam Formation was measured at the Branson Canyon section where it reaches a thickness of 25.5 m (Fig. 16). Elsewhere in the PTNM, the Apache Dam Formation reaches a thickness of 122 m (Lucas et al. 2015). It is composed of bedded algal limestone with black to dark grey chert nodules observed locally. Thin, reddish crinoid-rich limestone interbeds are present in the middle and upper parts of the exposed formation either side of Branson Canyon.

### Carnic Alps

The Garnitzenbach and Zottachkopf sections were measured along the Garnitzenklamm gorge and on the northern wall of the Trogkofel massif, respectively (Figs. 1, 15c). These sections are dominantly composed of bedded and massive limestone and minor sandstone of the Zweikofel, Zottachkopf and lowermost part of the Trogkofel formations (Figs. 2,

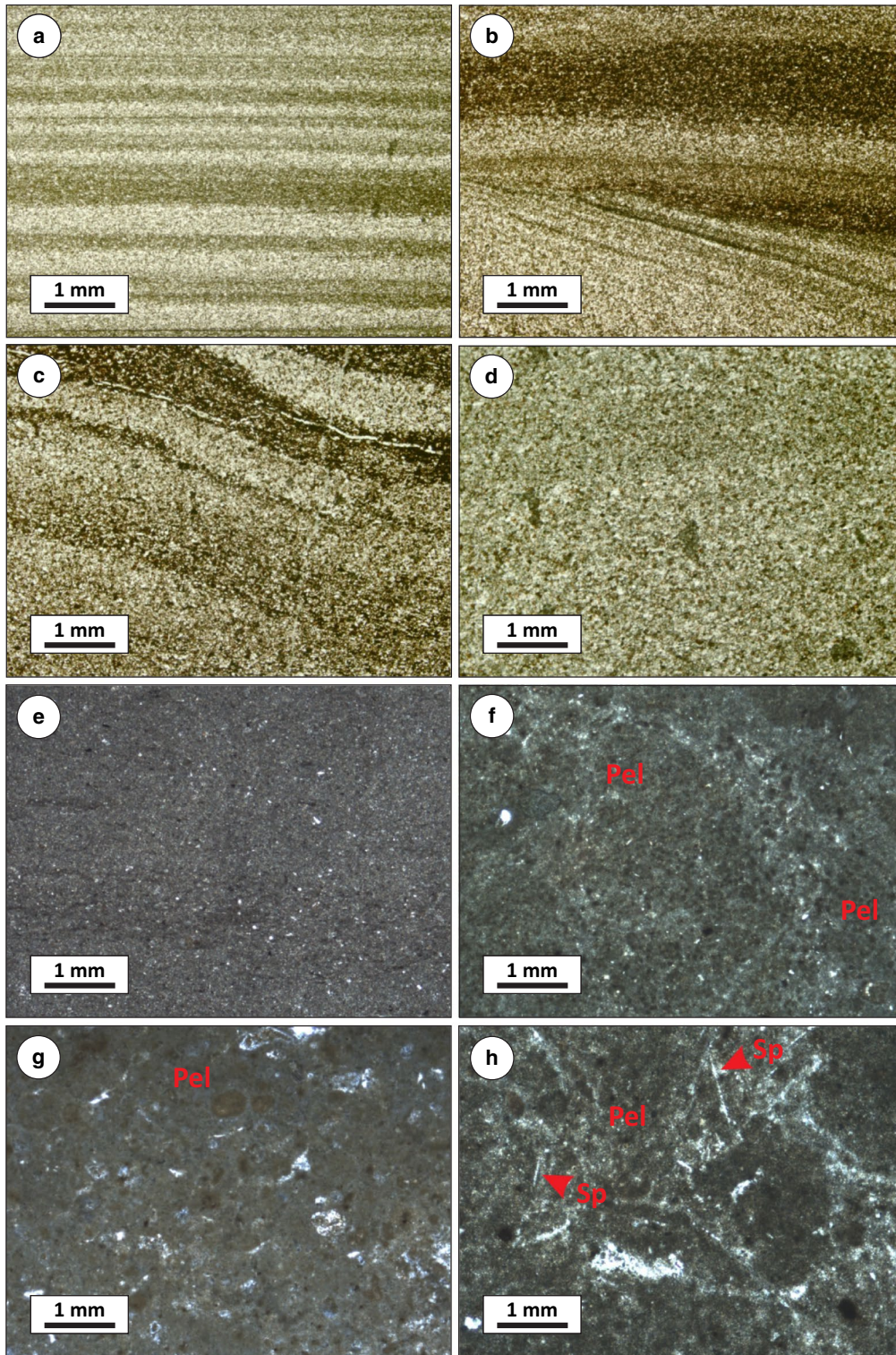


**Fig. 3** Photomicrographs of MF<sub>RM1</sub> (Siltstone to fine sandstone): **a–d** Parallel and cross-lamination in siltstone. MF<sub>RM2</sub> (Unfossiliferous mudstone): **e–h** Mudstone with abundant peloids (Pel), silt-sized quartz grains, and sponge spicules (Sp)

17). The Carnic Alps are a 140 km long mountain range located on the southern flank of the Central European Variscides straddling the Austrian-Italian border (Laufer et al.

2001). The European Variscides are part of the Variscan Belt, which formed by the collision between Laurussia and Gondwana during the Late Ordovician-Late Carboniferous

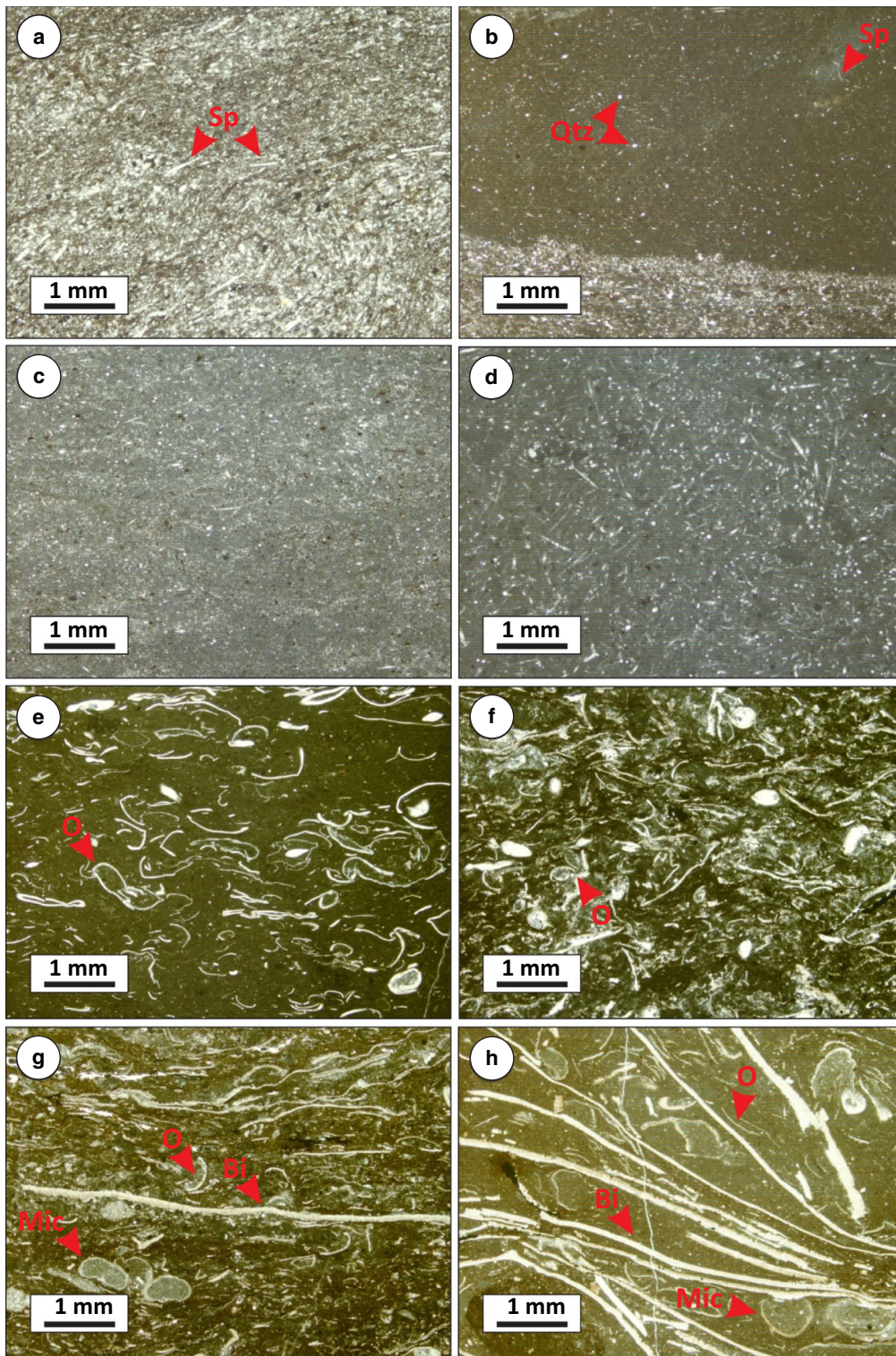


**Fig. 4** Photomicrographs of MF<sub>RM3</sub> (Spiculitic wackestone-packstone): **a** Packstone with abundant sponge spicules (Sp) showing a preferred depositional orientation. **b** View of a wackestone with variable amounts of sponge spicules (Sp) and rare quartz grains (Qtz) (above) and a packstone with abundant sponge spicules (below). **c–d**

Bioturbated packstone with abundant sponge spicules and silt-sized quartz grains. MF<sub>RM4A/B</sub> (Mollusc and ostracod wackestone-packstone): **e–f** Wackestone and packstone with abundant crushed ostracod shells (O). **g–h** Packstone with bivalve shells (Bi), microconchids (Mic) and ostracod shells (O)

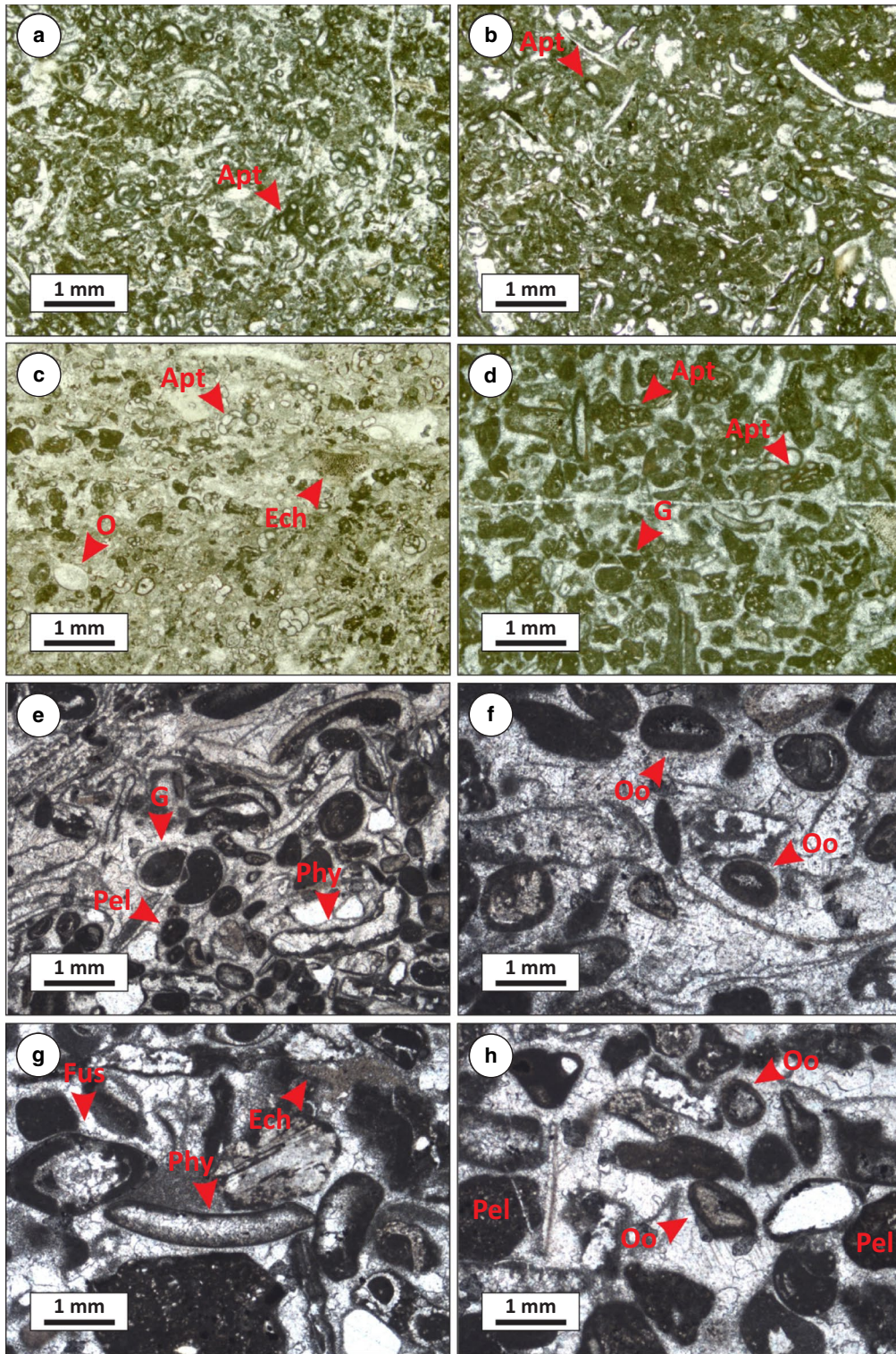


**Fig. 5** Photomicrographs of MF<sub>RM5</sub> (Encrusting foraminifer packstone): **a–d** Packstone and grainstone with abundant apterrinellid foraminifera (Apt) and common to rare ostracods (O), echinoderms (Ech) and gastropods (G). MF<sub>RM6</sub> (Ooid packstone-grainstone): **e–h**

Grainstone with abundant bioclasts of phylloid algae (Phy), gastropods (G), echinoderms (Ech), fusulinids (staffeloid) (Fus), ooids (Oo), peloids (Pel) and other grains

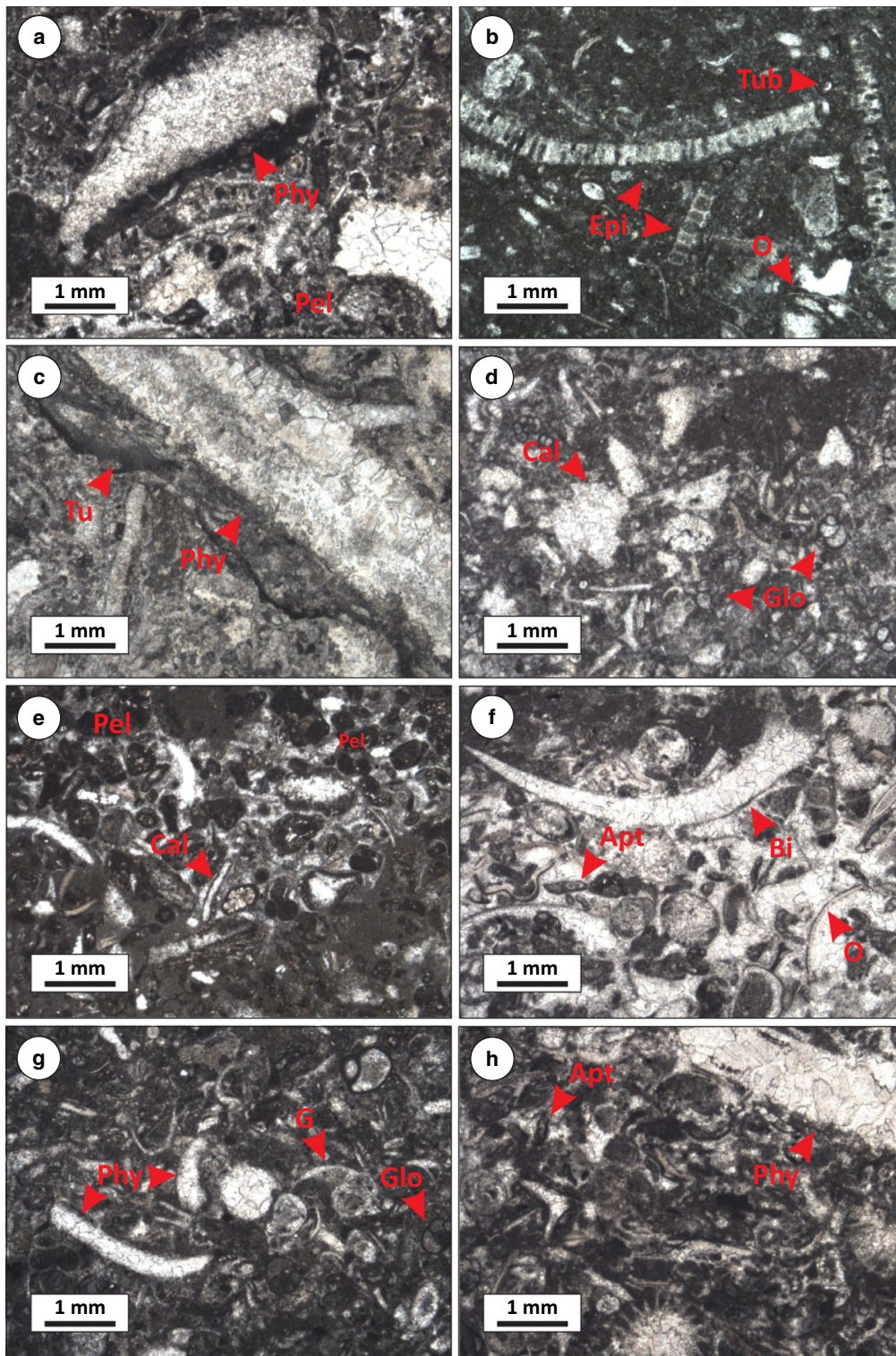


**Fig. 6** Photomicrographs of MF<sub>RM</sub>7A (Phylloid algal wackestone-packstone): **a–d** Packstone with broken plates of phylloid (Phy), epimastoporoid (Epi) and other calcareous (Cal) algae, globivalvulinids (Glo), ostracods (O), peloids (Pel), encrusting foraminifers (Tub) and

*Tubiphytes* (Tu). MF<sub>RM</sub>7B (Phylloid and epimastoporoid algal packstone-rudstone): **e–h** Packstone with abundant peloids (Pel), calcareous algae (Cal), encrusting foraminifers (Apt), gastropods (G), globivalvulinids (Glo), bivalves (Bi) and ostracods (O)

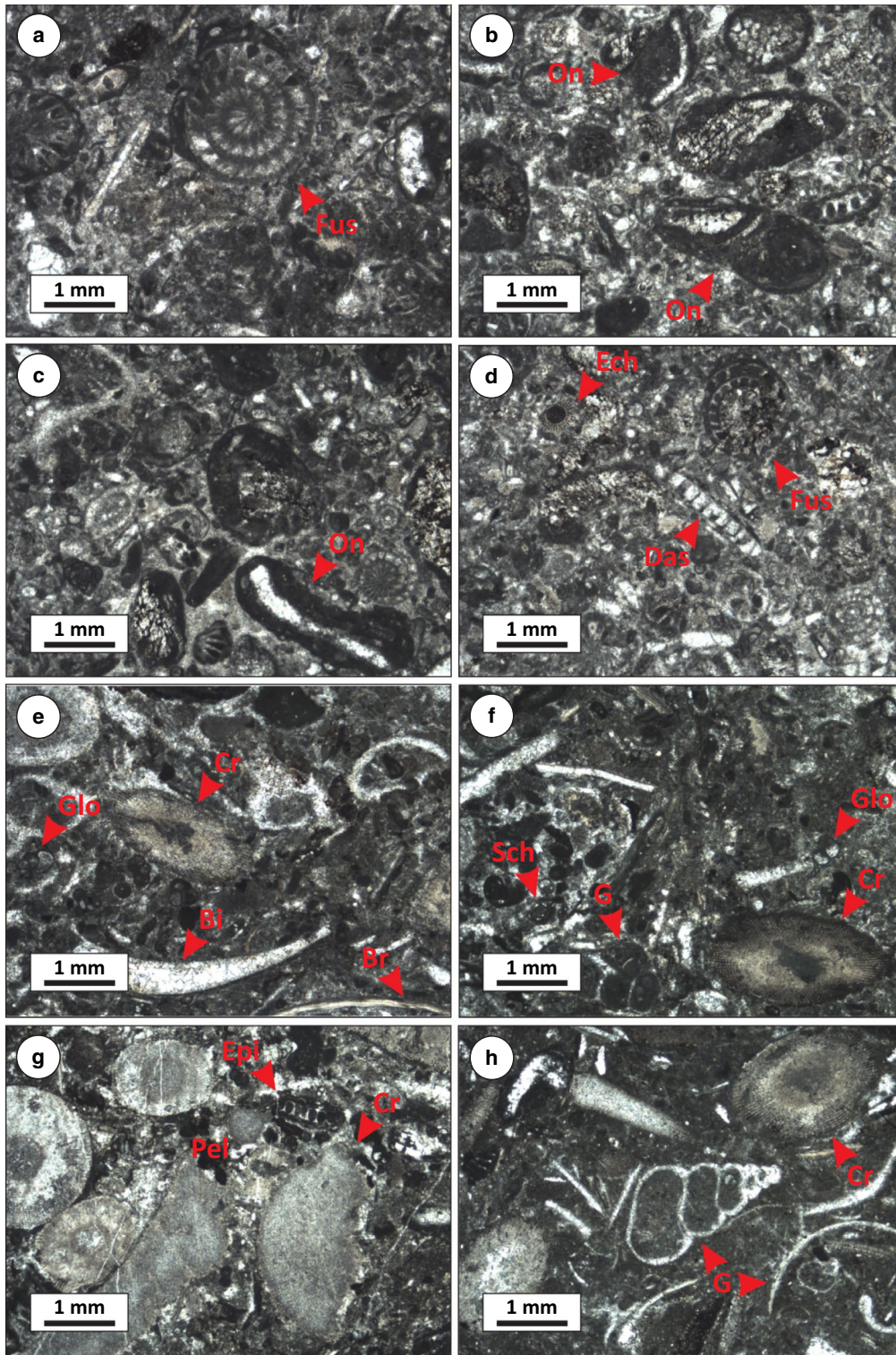


**Fig. 7** Photomicrographs of MF<sub>RM8</sub> (Oncoid and algal packstone): **a–d** Packstone with subrounded to oblong oncoids (On) with calcareous algae nuclei, fusulinids (Fus), echinoids (Ech) and dasyclad algae (Das). Other grains present include bryozoan fragments, peloids, small foraminifers, and ostracods. MF<sub>RM9</sub> (Algal, echinoderm and

small foraminifer packstone): **e–h** Packstone with abundant intact and broken crinoid ossicles (Cr), recrystallized broken bivalve shells (Bi), gastropods (G), globivalvulinids (Glo), brachiopod shells (Br) and other grains including epimastoporoid (Epi), small foraminifers (Sch) and peloids (Pel)

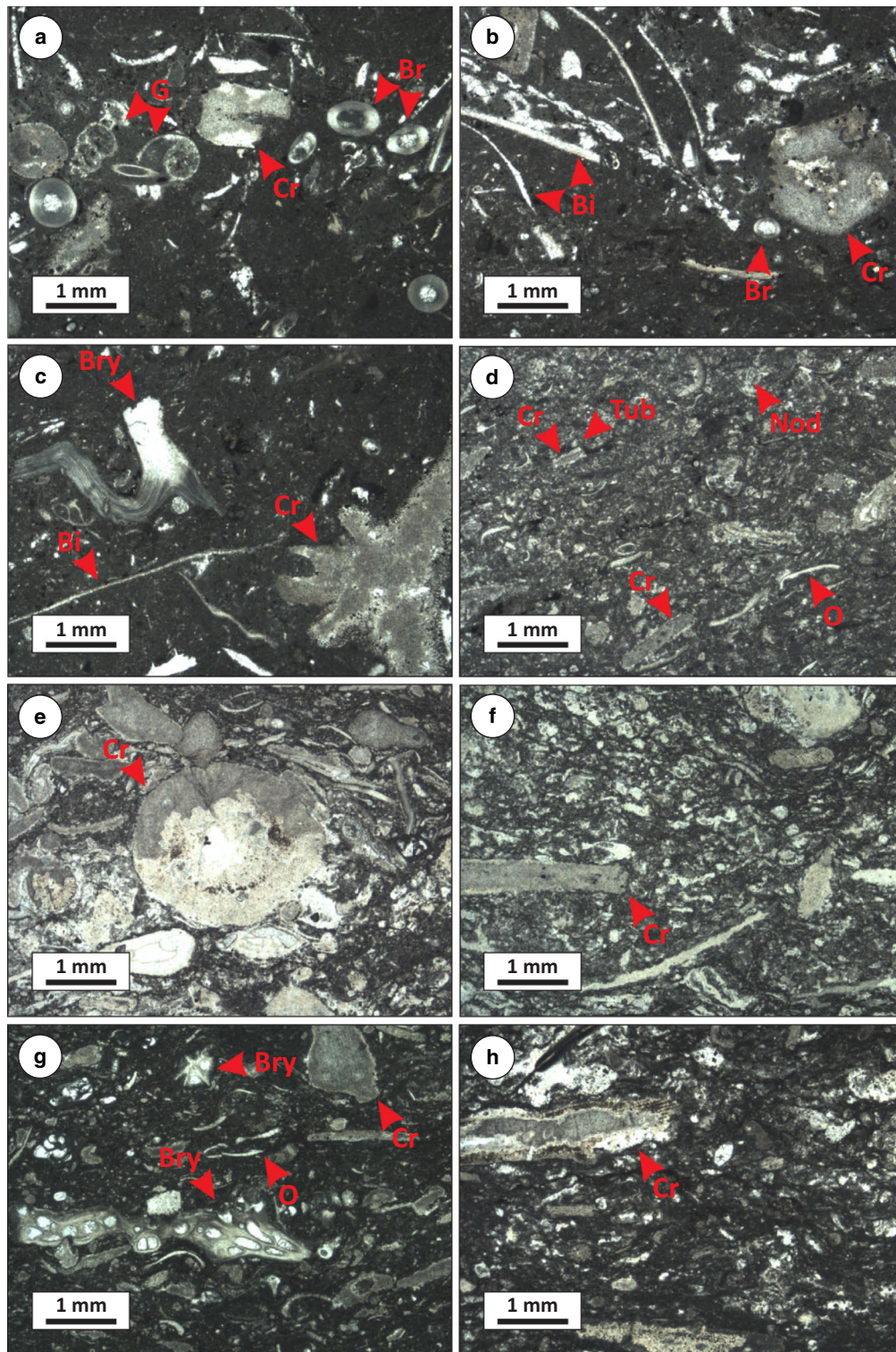


**Fig. 8** Photomicrographs of MF<sub>RM10</sub> (Echinoderm, peloid and small foraminifer packstone): **a–d** Packstone with broken and intact, rounded and pentagonal crinoid ossicles (Cr), gastropods (G), recrystallized bivalve fragments (Bi), oriented brachiopod spines (Br), ostracods (O), nodosariids (Nod) and encrusting foraminifers (Tub).

MF<sub>RM11</sub> (Laminated heterozoan packstone): **e–h** Packstone with abundant crinoid ossicles of various sizes (some are partially silicified) (Cr), broken fragments of ramose bryozoans (Bry), and broken and intact ostracod carapaces (O)

**Table 2** Description of the thirteen microfacies observed in the uppermost part of the Grenzland, Zweikofel, Zottachkopf and lowermost part of the Trogkofel formations in the Carnic Alps, southern Austria

Microfacies name	Allochem assemblage	Distribution	Depositional environment
MF <sub>CA</sub> 1 Siltstone to fine sandstone	Rare echinoderms, bivalves, bryozoans, brachiopods, nodosariids and lasiodiscids (Fig. 9a–d)	Uppermost part of the Grenzland Formation and Zweikofel formation	Inner ramp. Moderate to high-energy shoreface environment
MF <sub>CA</sub> 2 Mixed siliciclastic-carbonate packstone	Abundant common dasyclad algae. Common-rare bryozoans, brachiopods, echinoderms, globivalvulinids, encrusting foraminifers, ostracods, gastropods and phylloid and epimastoporoid algae (Fig. 9e–h)	Grenzland, Zweikofel, and lower half of the Zottachkopf formations	Inner ramp. Very shallow under medium to high energy conditions above FWWB
MF <sub>CA</sub> 3 Encrusting foraminifer packstone	Abundant encrusting foraminifers. Common epimastoporoid and phylloid algae, <i>Ellesmerella</i> , <i>Girvanella</i> , oncooids and ostracods (Fig. 10a–d)	Found in the Grenzland, Zweikofel, and Zottachkopf formations	Inner ramp. Below FWWB possibly a lagoon
MF <sub>CA</sub> 4 <i>Ellesmerella</i> and encrusting foraminifer wackestone-packstone	Abundant <i>Ellesmerella</i> . Common-rare encrusting foraminifers and dasyclad and phylloid algae (Fig. 10e–h)	Present in the Grenzland and Zweikofel formations	Inner ramp. Above and below the FWWB and above the thermocline, possibly in a lagoon
MF <sub>CA</sub> 5 Dasyclad algal packstone-grainstone	Abundant dasyclad algae. Common-rare epimastoporoid, encrusting foraminifers, phylloid algae, bivalves, <i>Girvanella</i> and oncooids (Fig. 11a–d)	Zweikofel and Zottachkopf formations	Inner ramp. Above and below the FWWB and above the thermocline
MF <sub>CA</sub> 6 Ooid packstone-grainstone	Abundant ooids and pisoids. Rare bivalves, fusulinids, echinoderms, apterrinellids, peloids, gastropods, <i>Tubiphytes</i> , lasiodiscids and dasyclad algae (Fig. 11e–h)	Observed in the Zweikofel formation	Inner ramp. Above FWWB and above the thermocline. Moderate to high energy conditions
MF <sub>CA</sub> 7 Bioclastic packstone-grainstone	Common phylloid, dasyclad algae, <i>Anthracoarella</i> , small foraminifers, <i>Tubiphytes</i> , oncooids, fusulinids, gastropods and echinoderms. Rare peloids, calcareous sponges, encrusting foraminifers and brachiopods (Fig. 12a–d)	Present in the Zweikofel and Zottachkopf formations	Inner ramp. At or above FWWB and above the thermocline. Moderate to high energy conditions

Table 2 (continued)

Microfacies name	Allochem assemblage	Distribution	Depositional environment
MF <sub>CA</sub> 8 Oncoid packstone-grainstone	MF <sub>CA</sub> 8A – Oncoid, fusulinid, calcareous algal p.-g.: Abundant-common oncoids, fusulinids, phylloid algae and echinoderms (Fig. 12e–h) MF <sub>CA</sub> 8B – Oncoid, fusulinid, echinoderm p.-g.: Abundant-common oncoids, fusulinids, bryozoans, dasyclad algae and <i>Ellesmerella</i> MF <sub>CA</sub> 8C – Oncoid, fusulinid, dasyclad algal p.-g.: Abundant-common oncoids, dasyclad algae, fusulinids and bryozoans MF <sub>CA</sub> 8D – Oncoid, encrusting foraminifer, echinoderm p.-g.: Abundant-common oncoids, encrusting foraminifers, echinoderms, dasyclad algae and peloids	Found in the Zweikofel and Zottachkopf formations	Mid ramp. At and below FWWB and above the thermocline. Moderate energy conditions
MF <sub>CA</sub> 9 <i>Anthracoporella</i> floatstone	Abundant <i>Anthracoporella</i> . Common encrusting foraminifers, <i>Ellesmerella</i> , <i>Tubiphytes</i> , echinoderms, <i>Neoanichodium</i> and calcareous sponges. Rare <i>Girvanella</i> and small foraminifers (Fig. 13a–c)	Observed in the Zweikofel and Zottachkopf formations	Mid ramp. Below FWWB and above the thermocline
MF <sub>CA</sub> 10 Calcareous algal packstone-floatstone	Abundant phylloid algae. Rare dasyclad algae, <i>Girvanella</i> , echinoderms, <i>Tubiphytes</i> , calcareous algae and small foraminifers (Figs. d–g)	Found in the Zweikofel and Zottachkopf formations	Mid ramp. Below FWWB and above the thermocline
MF <sub>CA</sub> 11 Fusulinid and echinoderm packstone-grainstone	Abundant fusulinids and echinoderms. Common-rare bryozoans, brachiopods, phylloid and epimastopoid algae and oncoids. Rare small and encrusting foraminifers, dasyclad algae and gastropods (Fig. 14a–d)	Only present in the Zweikofel formation	Mid ramp. Below FWWB and above the thermocline
MF <sub>CA</sub> 12 Echinoderm and bryozoan wackestone-packstone	Abundant echinoderms. Common-rare bryozoans and nodosariids. Rare fusulinids, trilobites, small and encrusting foraminifers, phylloid algae and oncoids (Fig. 14e–f)	Observed in the Zweikofel and Zottachkopf formations	Mid ramp. Below FWWB and below the thermocline
MF <sub>CA</sub> 13 <i>Tubiphytes</i> , bryozoan, algal boundstone	Abundant <i>Tubiphytes</i> , phylloid algae, peloids and <i>Girvanella</i> . Common-rare echinoderms, dasyclad algae and encrusting foraminifers. Rare small foraminifers, brachiopods, fusulinids and <i>Cuneiphyucus</i> (Fig. 14g–h)	Found in the Zottachkopf and Trogkofel formations	Mid ramp. Below FWWB and below the thermocline

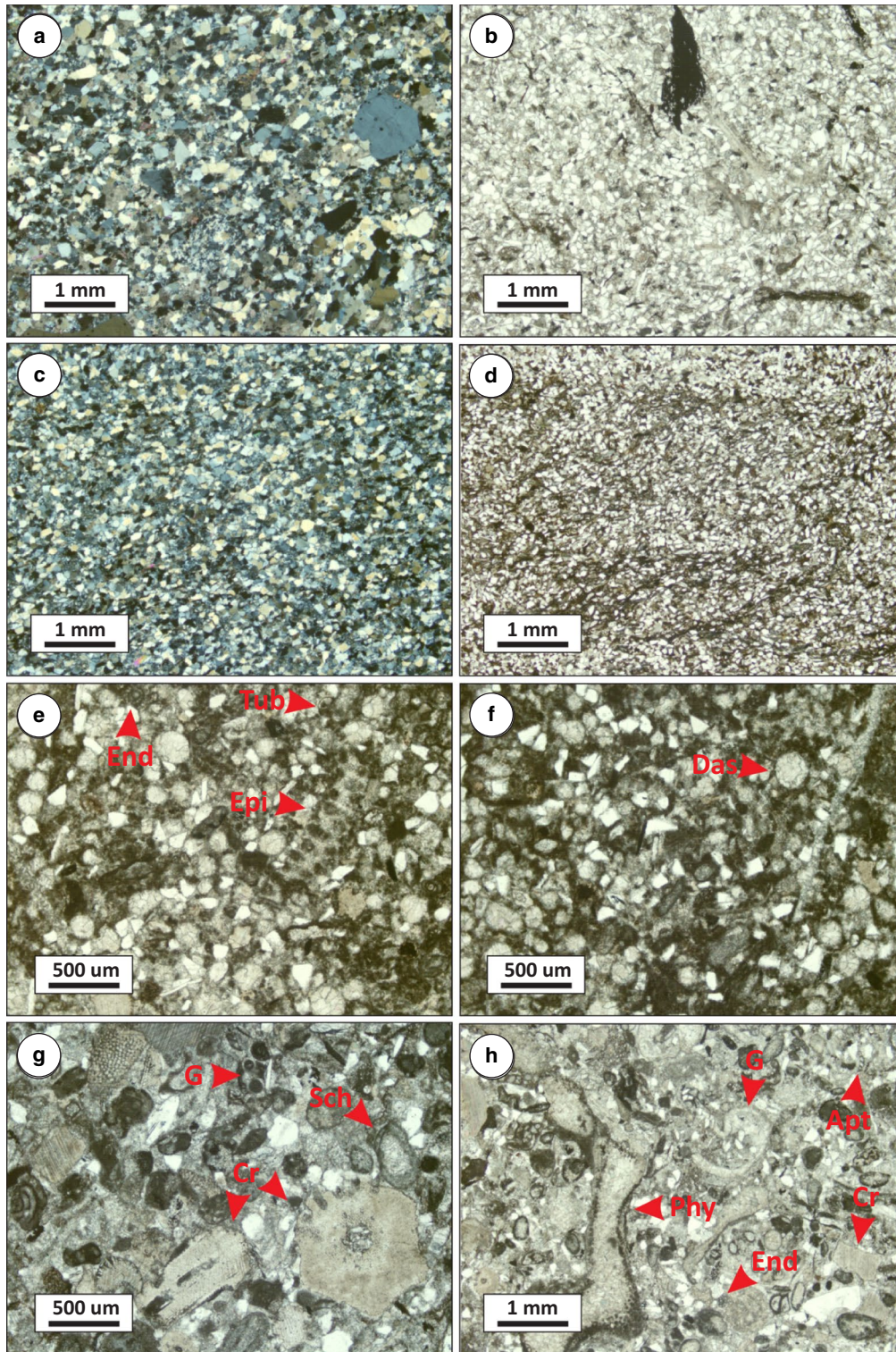


**Fig. 9** Photomicrographs of MF<sub>CA1</sub> (Siltstone to fine sandstone): **a** Moderately sorted sandstone composed of fine, medium and coarse angular to sub-angular quartz grains in cross polarized light (XPL). **b** Fine sand grains, clay minerals, organic matter and rare grains in plane polarized light (PPL). **c–d** Sub-rounded to sub-angular, well-sorted fine and very fine quartz grains in XPL and PPL. Bioturbation

observed in photomicrographs. MF<sub>CA2</sub> (Mixed siliciclastic-carbonate packstone): **e–h** Fine, sub-rounded to sub-angular quartz grains, dasyclad (Das), epimastoporoid (Epi), and phylloid (Phy) algae broken fragments, tubertinids (Tub), apterrinellids (Apt), gastropods (G), crinoid ossicles (Cr), endothyrids (End) and small foraminifers (Sch) in PPL

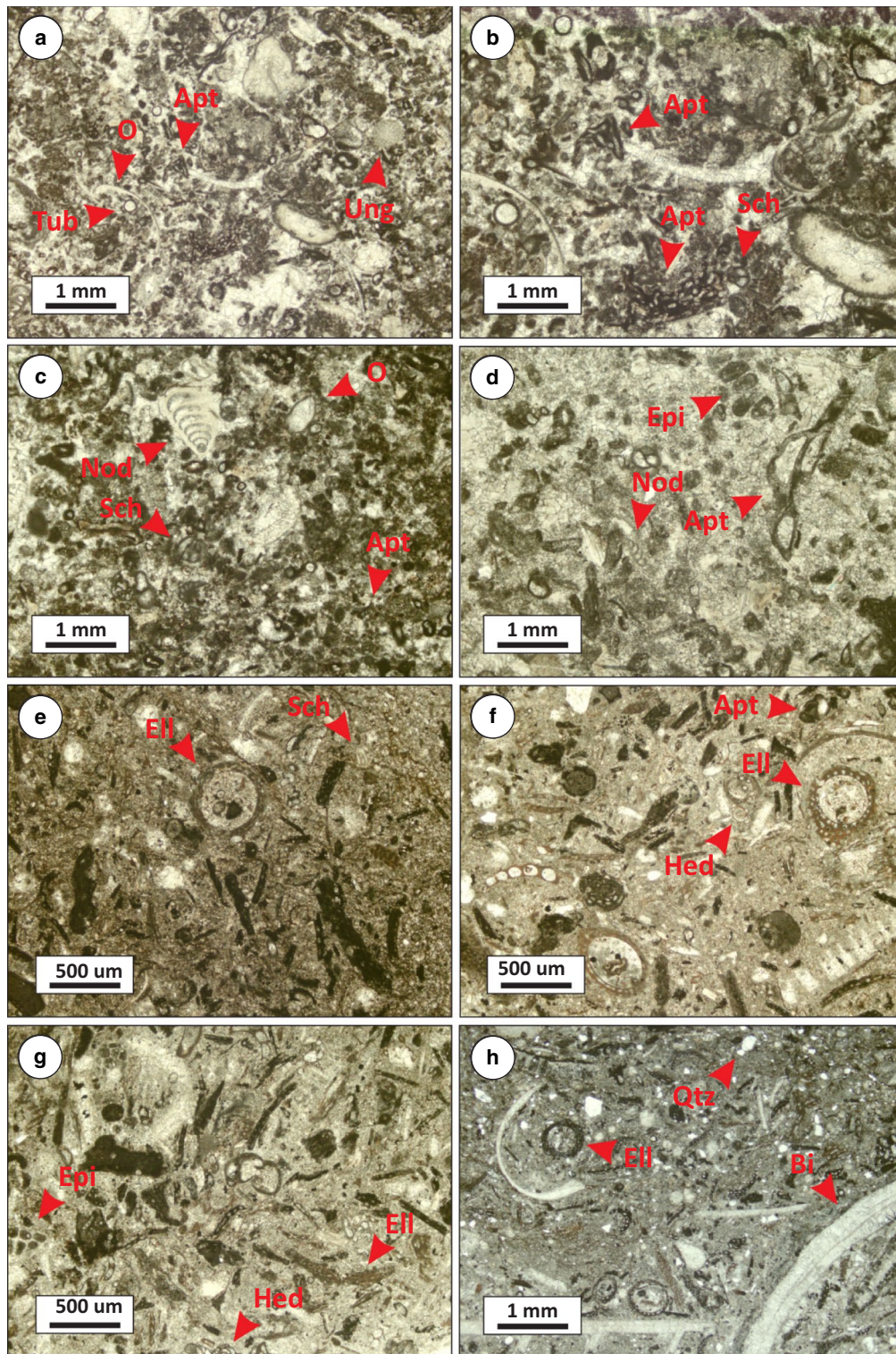


**Fig. 10** Photomicrographs of MF<sub>CA</sub>3 (Encrusting foraminifer packstone): **a** General view showing abundant apterrinellids (Apt), and rare tuberitids (Tub), ungdarellid algae (Ung), and ostracods (O) in a packstone. **b–d** Detailed images showing abundant apterrinellids (Apt), small foraminifers (Sch), epimastoporoid algae (Epi), nodosariids (Nod) and ostracods (O). MF<sub>CA</sub>4 (*Ellesmerella* and encrusting

foraminifer wackestone-packstone): **e–h** Abundant broken and intact fragments of *Ellesmerella biomurae* (Ell). Based on the shape of the substrate where *Ellesmerella* was encrusted it may display a circular, oblong or straight morphology. Quartz grains (Qtz), apterrinellids (Apt), bivalves (Bi), *Hedraites* (Hed) and epimastoporoid algae (Epi) are also observed

(Franke 1989). The Carnic Alps are composed of a Late Ordovician-Devonian continuous pre-orogenic sedimentary succession followed by a succession of south-verging nappes stacked during the Variscan Orogeny in the Mississippian (Laufer et al. 2001). Late Ordovician-Mississippian strata are referred to as the Variscan basement. Pennsylvanian to Permian units deposited in successor basins sit unconformably on Variscan basement rocks (Laufer et al. 2001). In the study area, the Variscan basement comprises Devonian limestone, lower Carboniferous flysch deposits and basaltic pillow lavas of unknown age of the Hochwipfel nappe (Laufer et al. 2001; Krainer and Davydov 1998; Schaffhauser 2013). Above these strata, the post-Variscan succession reaches a thickness of more than 2000 m and is composed of the Bombaso Formation followed by strata of the Auernig, Rattendorf and Trogkofel groups (Krainer et al. 2019). The Bombaso Formation is composed of syn-tectonic breccias and immature conglomerate, sandstone, shale, limestone and volcanic rocks deposited during the initial opening of the successor Pramollo Basin (Krainer and Davydov 1998; Davydov and Krainer 1999). The overlying Auernig Group sits conformably above the Bombaso Formation and comprises cyclic clastic and carbonate units of the Meledis, Piz-zul, Corona, Auernig and Carnizza formations (Krainer and Davydov 1998). The Auernig Group is conformably overlain by the Rattendorf Group (Fig. 2). This group is composed of cyclic carbonate and clastic strata of the Schulterkofel, Grenzland and Zweikofel formations, and non-cyclic strata of the Zottachkopf Formation. The Schulterkofel Formation is composed of shallow-marine bedded limestone, marl interbeds, and thin siliciclastic intervals divided into three depositional sequences. *Anthracoporella* mounds of up to 22 m thick punctuate the formation (Samankassou 1999). At its type locality, the Schulterkofel reaches a thickness of 155–160 m (Forke et al. 1998; Krainer et al. 2019). The Grenzland Formation conformably overlies the Schulterkofel and comprises a succession of shallow-marine siliciclastic units interbedded with thin limestone lenses (Krainer et al. 2019). According to Krainer et al. (2019), the Grenzland Formation exceeds a thickness of 300 m and displays cyclic and non-cyclic siliciclastic intervals. The Zweikofel Formation sits conformably on top of the Grenzland Formation and reaches a maximum thickness of 170 m. The Zweikofel Formation is comprised of cyclic, well-bedded limestone units with rare thin clastic intervals composed of conglomerate, sandstone and siltstone (Forke et al. 1998).

The stratigraphic relationship between the Zweikofel and Zottachkopf formations remains a source of debate. Schaffhauser et al. (2010) officially introduced the lithostratigraphic unit, Zottachkopf Formation, to refer to the well-bedded, red-coloured limestone rich in oncoids, ooids and algal mounds located at the north and south walls of the Trogkofel and Zottachkopf massifs. These rocks are

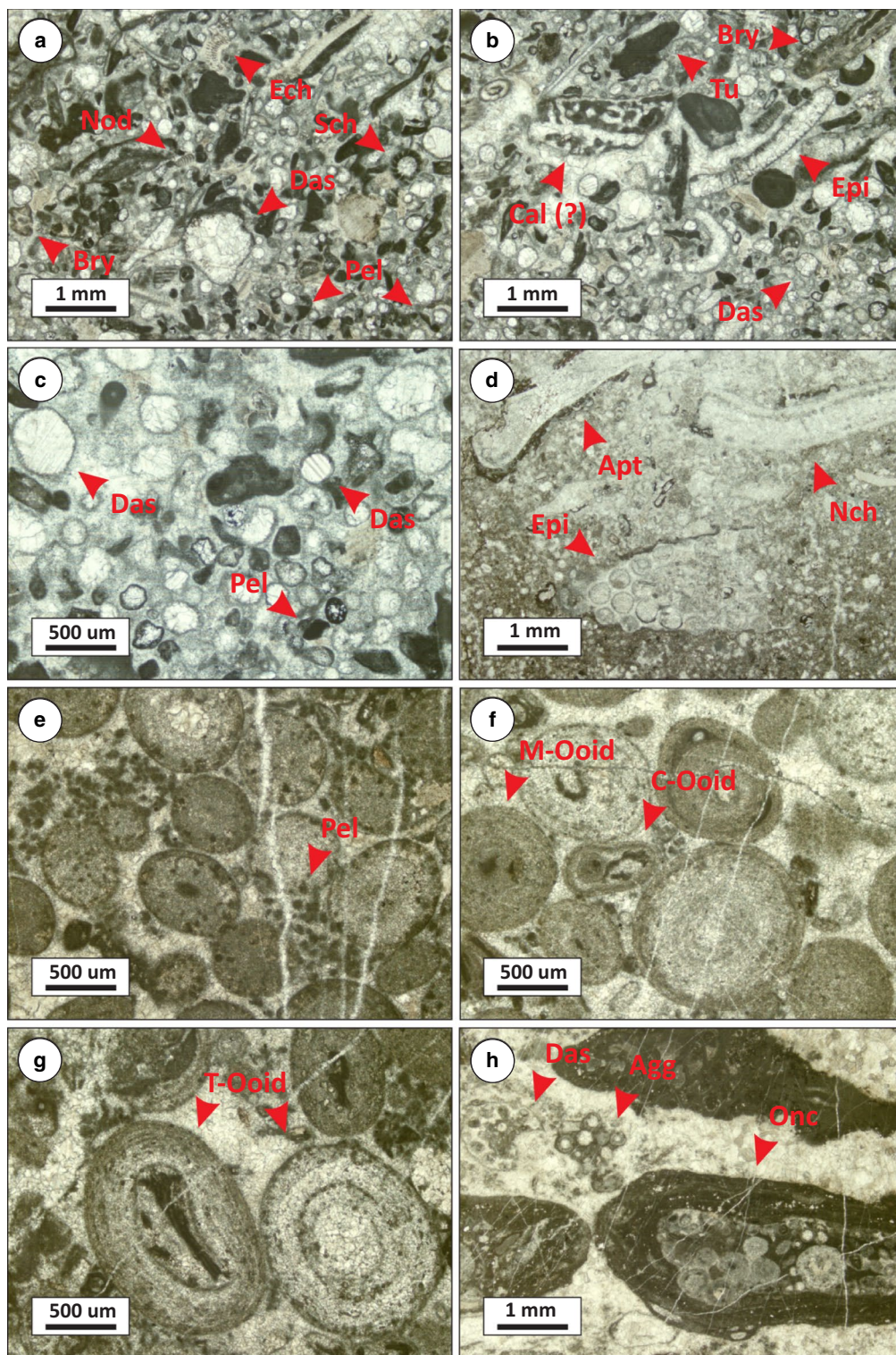
interpreted to correlate with the red-coloured limestone beds of the ‘Höhe 2004’ locality sited approximately 1 km to the east of the Trogkofel massif. The Zottachkopf Formation is widely interpreted as non-cyclic. Both the Zweikofel and Zottachkopf formations are overlain by the Trogkofel Limestone of the Rattendorf Group. The contact between the Zweikofel and Trogkofel formations in the Garnitzenklamm gorge and the Zweikofel massif is erosional and disconformable (Krainer et al. 2019). Locally, limestone breccias with a Zweikofel affinity overlie this contact in the Zweikofel massif (Krainer et al. 2009). At the Trogkofel massif the contact between the Zottachkopf Formation and the Trogkofel Limestone is conformable, and it is represented by a sharp transition between well-bedded to massive limestone units. The Trogkofel Limestone is the oldest unit of the Rattendorf Group. It is composed of massive limestone at Garnitzenklamm and the Trogkofel massif. At Zweikofel, the Trogkofel Limestone is composed of a basal massive limestone unit interbedded with carbonate breccias and an overlying marl unit (“Sonderfazies”), followed by a massive limestone unit with north-verging clinofolds (Krainer et al. 2019).

## Cyclicity in the Cisuralian successions of the Robledo Mountains and the Carnic Alps

### Cyclicity in the Robledo Mountains

#### Low-frequency sequences

The upper part of the Community Pit, Robledo Mountains and lower Apache Dam formations in the Robledo Mountains are herein divided into three low-frequency sequences (Fig. 16). The upper part of the Community Pit Formation at the Flood section is interpreted as the first complete low-order sequence in the succession. At Flood, Community Pit strata overlie a Cenozoic sill also found atop of the lower interval of the formation at Monument North, where the exposed formation reaches a thickness of 52.8 m (Lucas et al. 2015). Hence, the total thickness of the Community Pit Formation in the Robledo Mountains may reach up to 157 m providing no strata are lost between the Monument North and Flood sections. Lucas et al. (2015) measured a complete section of the Community Pit Formation at Indian Springs Canyon (ISC) with a thickness of 92.6 m. Based on the facies reported by these authors at that location and at Monument North, the entire Community Pit Formation is herein divided into two low-frequency sequences. The lower contact of the lower sequence is interpreted as above an ooid-rich limestone unit in the uppermost part of the Shalem Colony Formation at ISC and at the base of its correlative conglomerate unit at Monument North illustrated by Lucas et al. (2015).



The MFS of this sequence is tentatively placed within Bed 135 at ISC due to the reported presence of fusulinids, which may be evidence of deeper, open-marine conditions. The upper contact of the sequence is interpreted at the base of Bed 151 at ISC, composed of sandstone and conglomeratic sandstone that scours into the underlying dolomitic bed (S.

Lucas, pers. comm. April 21, 2022). At Monument North, microfacies illustrated by Lucas et al. (2015) are indicative of a subtidal, open-marine setting and a restricted subtidal to intertidal environment in the middle and uppermost intervals of the section, respectively. These microfacies may support the presence of a low-frequency, T-R sequence in the

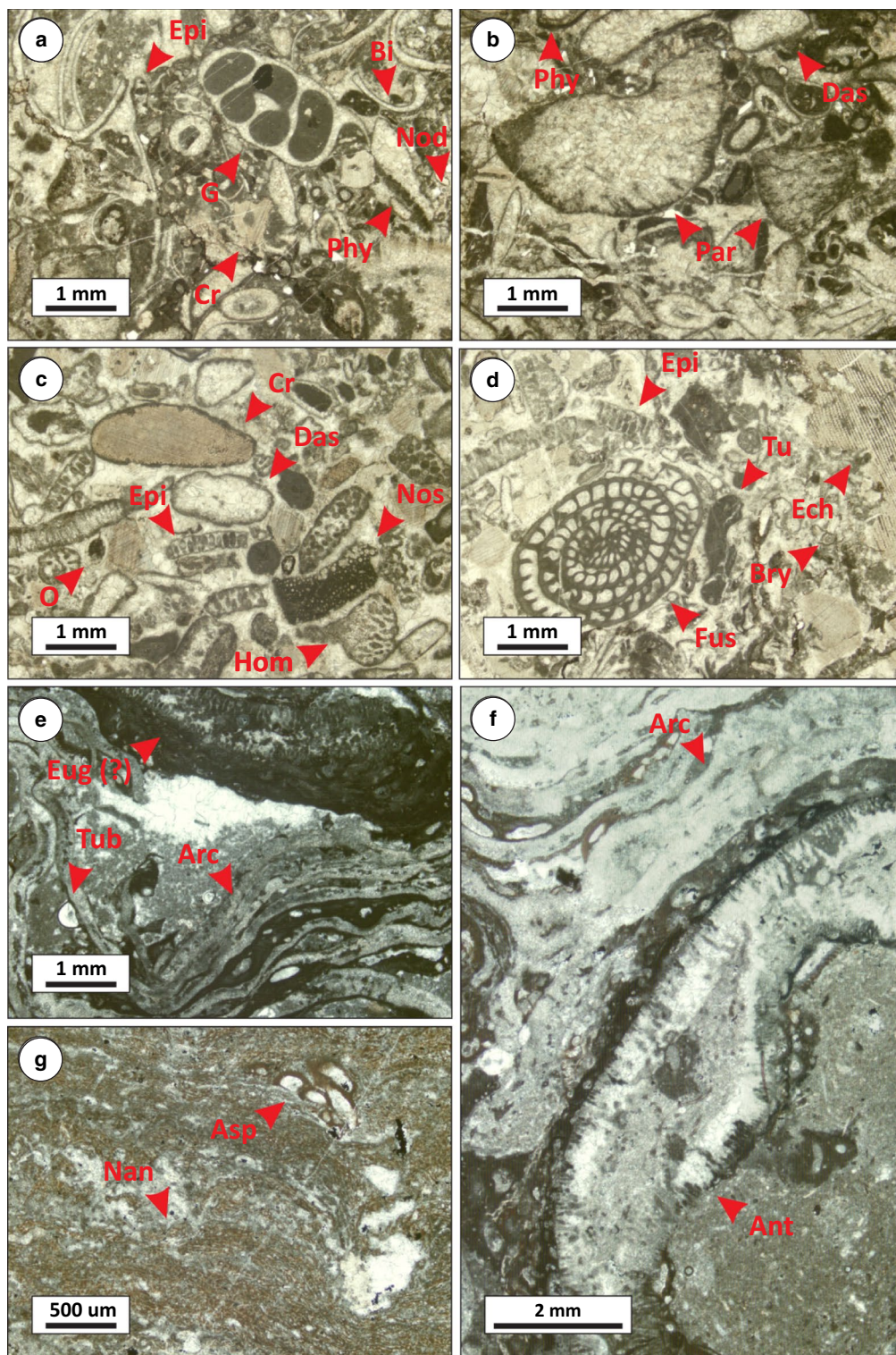
**Fig. 11** Photomicrographs of MF<sub>CA</sub>5 (Dasyclad algal packstone-grainstone): **a** Broken and abraded fragments of dasyclad algae (Das). Note the lack of internal structures due to recrystallization during diagenesis. Broken fragments of echinoids (Ech) and bryozoans (Bry), nodoserids (Nod), small foraminifers (Sch) and peloids (Pel) are also present. **b** Abundant fragments of dasyclad algae (Das) along with epimastoporoid algae (Epi), *Tubiphytes* (Tu), bryozoans (Bry) and potentially *Calcipaterra* (Cal). **c** Detail image of abraded dasyclad (Das) fragments and peloids (Pel). **d** Unbroken talli of *Neoanchicodium* (Nch) encrusted by apterrinellids (Apt). Relatively well-preserved of plate of epimastoporoid (Epi) is also observed. MF<sub>CA</sub>6 (Ooid packstone-grainstone): **e** Detail image showing micritized (M-Ooid) and radial ooids with calcite cement and peloids (Pel) in the matrix (PPL). **f** Detail image of a deformed composite-ooid (C-Ooid) and various micritized ooids (M-Ooid) in a grainstone (PPL). **g** Tangential ooids (T-Ooid) with incipient recrystallization and micritization in cortex (PPL). **h** Dasyclad algae (Das), aggregates (Agg) and oncoids (Onc) were also observed in some samples of this microfacies (PPL)

lower part of the Community Pit Formation. Despite this evidence, further detailed petrographic analyses in the lower half of the formation are needed to confirm the presence of a low-frequency sequence. At Flood, the base of an incised fluvial channel located at 17 m, is interpreted as the upper contact of the aforementioned lower sequence, and as the base of the second low-frequency sequence observed in the studied succession (Figs. 16, 18a). Above this boundary, a deepening-upward trend is observed throughout the lower third of the formation. At the base of the sequence, the channel fill is composed of a succession of conglomerate, micritic limestone, gypsiferous limestone, and abundant plant fossils and tree trunk remains that has been interpreted as the result of base-level rise (Lang et al. 2015). Above the channel, a grain assemblage composed of abundant to common ooids, monaxon sponge spicules, ostracods, phylloid algae, echinoderms and small foraminifers is interpreted as the transgressive systems tract of the sequence (Figs. 4e–h, 16). This assemblage, which is characteristic of a proximal, shallow-water and low-energy subtidal environment, is progressively replaced by a distal, open-marine assemblage comprising abundant to common echinoderms, fusulinids, phylloid algae and *Tubiphytes* at 48.4–48.6 m (Figs. 7a–d, 16). The MFS of this sequence is placed at 48.6 m due to the presence of an open-marine, highly diversified fossil association (Figs. 7e–h, 16). Above the MFS, a shallowing-upward trend is observed in the upper two-thirds of the Community Pit Formation. The aforementioned highly diversified fossil assemblage is progressively replaced by an assemblage composed of peloids, sponge spicules, ostracods, microconchids and bivalves characteristic of shallow, semi-restricted inner-shelf settings followed by a unit of red supratidal sandstone, siltstone and shale (Figs. 3e–h, 4e–h, 16, 18b). The upper sequence boundary of this sequence is interpreted at the base of a 90 cm limestone bed in the lowermost part of the Robledo Mountains Formation at Branson Canyon located

above a palaeosol unit at 10.9 m (Fig. 18c). The bulk of the Robledo Mountains Formation is interpreted as the second complete low-frequency sequence observed in the Robledo Mountains (Fig. 16). Following its lower boundary, a TST displaying a deepening-upward trend is observed. The MFS is placed within the 83.8–88.2 m interval due to the presence of a heterozoan fossil assemblage with very abundant brachiopods, and abundant to common echinoderms, globivalvulinids and molluscs likely deposited in an open-marine setting at or below the thermocline (Figs. 7e–h, 16, 18d). Above this interval, a shallowing-upward RST is observed in the upper 33 m of the Robledo Mountains Formation. The limestone composed of a heterozoan fossil assemblage present at the MFS is progressively replaced by sandstone and siltstone, with abundant cross-lamination, asymmetric and climbing ripples, and soft-sediment deformation, likely deposited in fluvial channels on a tidal flat (Figs. 16, 18e). The upper sequence boundary of the sequence is the unconformable erosional contact between the Robledo Mountains and Apache Dam formations. The lower part of the Apache Dam Formation is interpreted as an incomplete low-frequency sequence (Fig. 16). The lower boundary of this sequence corresponds to the Robledo Mountains–Apache Dam erosional contact previously described. The lower two thirds of the exposed Apache Dam Formation is composed of a deepening-upward trend comprising a highly diversified fossil assemblage rich in phylloid and dasyclad algae, echinoderms, small and encrusting foraminifers, and peloids (Figs. 5e–h, 6a–h, 16). The MFS is placed at a resistant limestone bed composed of a fossil assemblage with abundant echinoderms, bryozoans and ostracods likely deposited below the thermocline and located at 141.7 m (Figs. 8e–f, 16). The upper third of the formation is interpreted as an incomplete RST that displays a shallowing-upward trend (Fig. 16).

### High-frequency sequences

**Community Pit Formation** Two incomplete (CP1 and CP4) and two complete (CP2 and CP3) high-frequency sequences were interpreted in the upper part of the Community Pit Formation at the Flood section (Fig. 16). Only the upper 17 m of the first sequence (CP1) outcrops at this location. It is composed of mudstone and packstone rich in siliceous monaxon sponge spicules, peloids, silt, common to rare ostracods, bivalves, gastropods and small foraminifers, and shale interbeds. This succession, interpreted as a restricted subtidal to supratidal environment due to the fossil content and the presence of fenestral fabric, is partially carved by a fluvial channel that expands laterally approximately 140 m (Fig. 18a) (Lang et al. 2015). The second sequence (CP2) is 21.5 m thick (17–38.5 m). The TST of this sequence (17–18.9 m) yields a fossil assemblage composed of abundant



to common echinoderms, brachiopods, bryozoans, phylloid algae, ostracods, ooids and small foraminifers (Figs. 16, 18f). This assemblage is indicative of a well-oxygenated open-marine setting under normal salinity conditions below FWFB and above the thermocline. It represents the first open-marine environment recorded in the Flood section. The

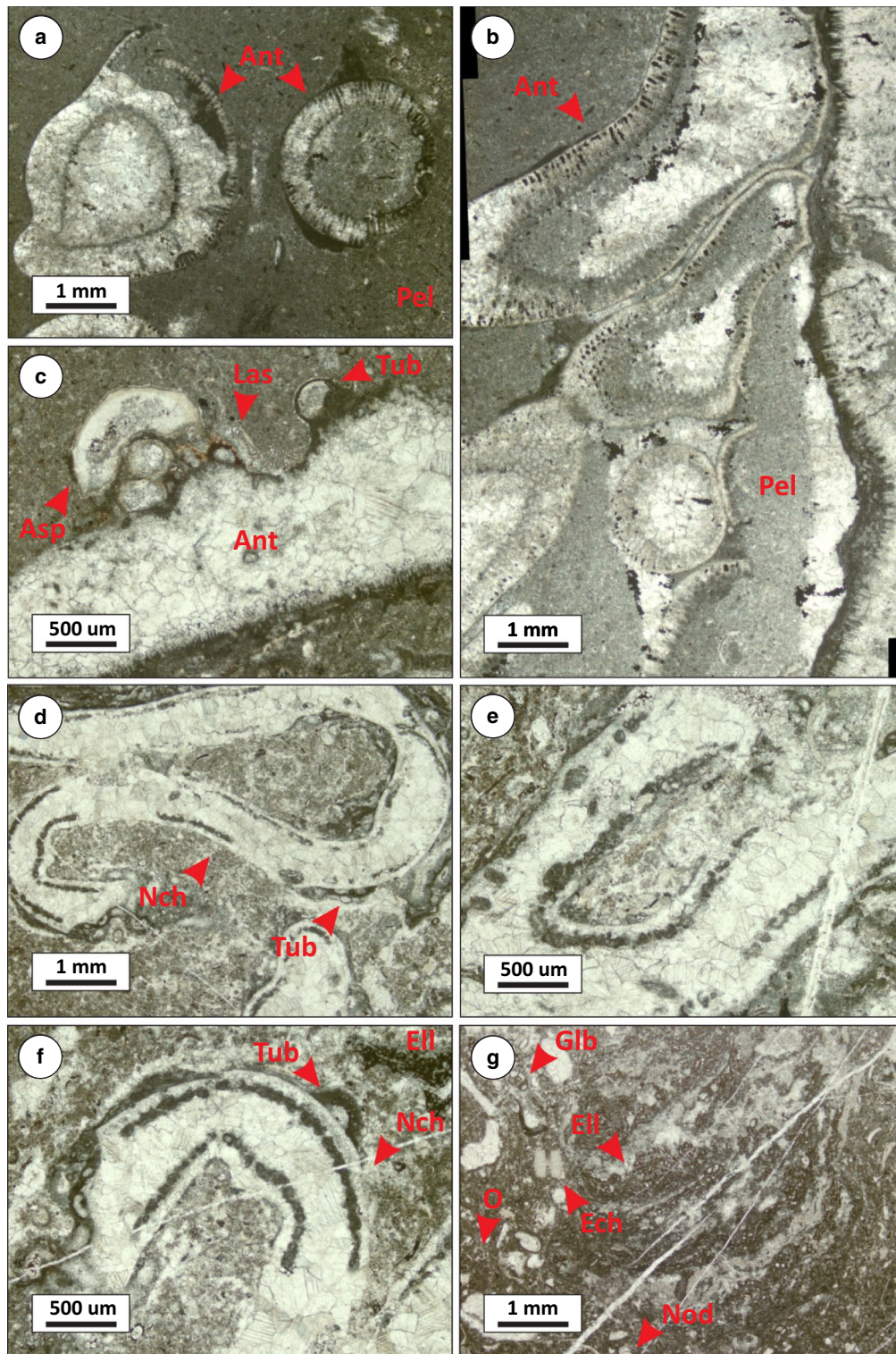
TST is then followed by an RST (18.9–38.5 m) composed of interbedded limestone and green to buff coloured shale beds with local dark brown chert nodules (Figs. 16, 18g). The RST displays a recurring shift between two distinctive fossil assemblages. The first assemblage comprises dominant siliceous sponge spicules and abundant peloids and is

**Fig. 12** Photomicrographs of MF<sub>CA</sub>7 (Bioclastic packstone-grainstone): **a** High diversity fossil assemblage containing gastropods (G), epimastoporoid (Epi) fragments, nodoserids (Nod), crinoids (Cr), bivalves (Bi) and fragments of phylloid algae (Phy) in PPL. **b** Abundant dasyclad (Das), phylloid (Phy) and partially recrystallized *Parachaetetes* (Par) in a packstone-grainstone (PPL). **c** Broken fragments of dasyclad (Das) and epimastoporoid (Epi) algae displaying a micritic envelope around the grains, crinoid fragments (Cr), ostracods (O), *Homannisiphon* (Hom) and *Nostocites* (Nos) in a grainstone (PPL). **d** Broken fragments including epimastoporoid algae (Epi), echinoderms (Ech), bryozoans (Bry), *Tubiphytes* (Tu) and a fusulinid (Fus) in a grainstone (PPL). MF<sub>CA</sub>8 (Oncoid packstone-grainstone): **e** Detail image of an oncolitic encrustation composed of tuberitids (Tub) and *Archaeolithophyllum* (Arc). An *Eugonophyllum* (Eug) plate is also observed encrusted by *Tubiphytes* and encrusting foraminifers. The geopetal fabric in the centre of the picture is composed by peloids (below) and spar calcite cement (above) (PPL). **f** Micropanorama of an oncolitic encrustation of an *Anthracoporella* plate (Ant). The encrustation is mainly composed of *Archaeolithophyllum* (Arc) and encrusting foraminifers (PPL). **g** Detailed images of the cortex of an oncolite composed of *Nansenella* (Nan) and the epibiont *Asphaltina* (Asp) (PPL)

herein interpreted as a semi-restricted environment below FWWB and above the thermocline (Fig. 4a–d). The second assemblage is composed of phylloid algae, encrusting foraminifers, small foraminifers, fusulinids, echinoderms, bryozoans, bivalves, gastropods and oncoids (Fig. 6e–h). This assemblage is interpreted as an open-marine environment between FWWB and the thermocline under euphotic conditions. The alternation between these assemblages may be the result of higher frequency glacioeustatic sequences nested within this cyclothem. The third sequence (CP3) is 36.9 m thick (38.5–75.4 m) (Fig. 16). Its TST (38.5–48.6 m) is composed of common to abundant echinoderms, fusulinids, phylloid and dasyclad algae, *Tubiphytes*, ostracods and encrusting foraminifers (Fig. 7e–h). The TST is overlain by a relatively thick RST composed of medium-thick, well-bedded grey fossiliferous limestone alternating with covered intervals that range between 1.1 and 3 m in thickness. Buff-coloured shale is observed within some covered intervals in the upper part of the cyclothem. Overall, the fossil assemblage of the RST is characterized by a highly diversified photozoan association composed of abundant to common echinoderms, fusulinids, small foraminifers, calcareous green algae and bivalves (Fig. 5a–h). This assemblage is indicative of a relatively deep, open-marine environment within the photic zone, located below FWWB and above the thermocline. A poorly diversified fossil assemblage composed of sponge spicules and ostracods is observed at 50.3 m and between 73.6 and 74.5 m at the base of the RST and the cyclothem top, respectively (Figs. 4e–h, 16). These strata are interpreted as a semi-restricted environment similar to samples on intervals 9.8–13, 20.1, 22.1, and 26.3 m (Fig. 16). The fourth sequence (CP4) is 28.5 m thick (75.4–103.9 m) at the Flood section and its continuation is 10.9 m thick (0–10.9 m) at Branson Canyon section (Fig. 16). Its

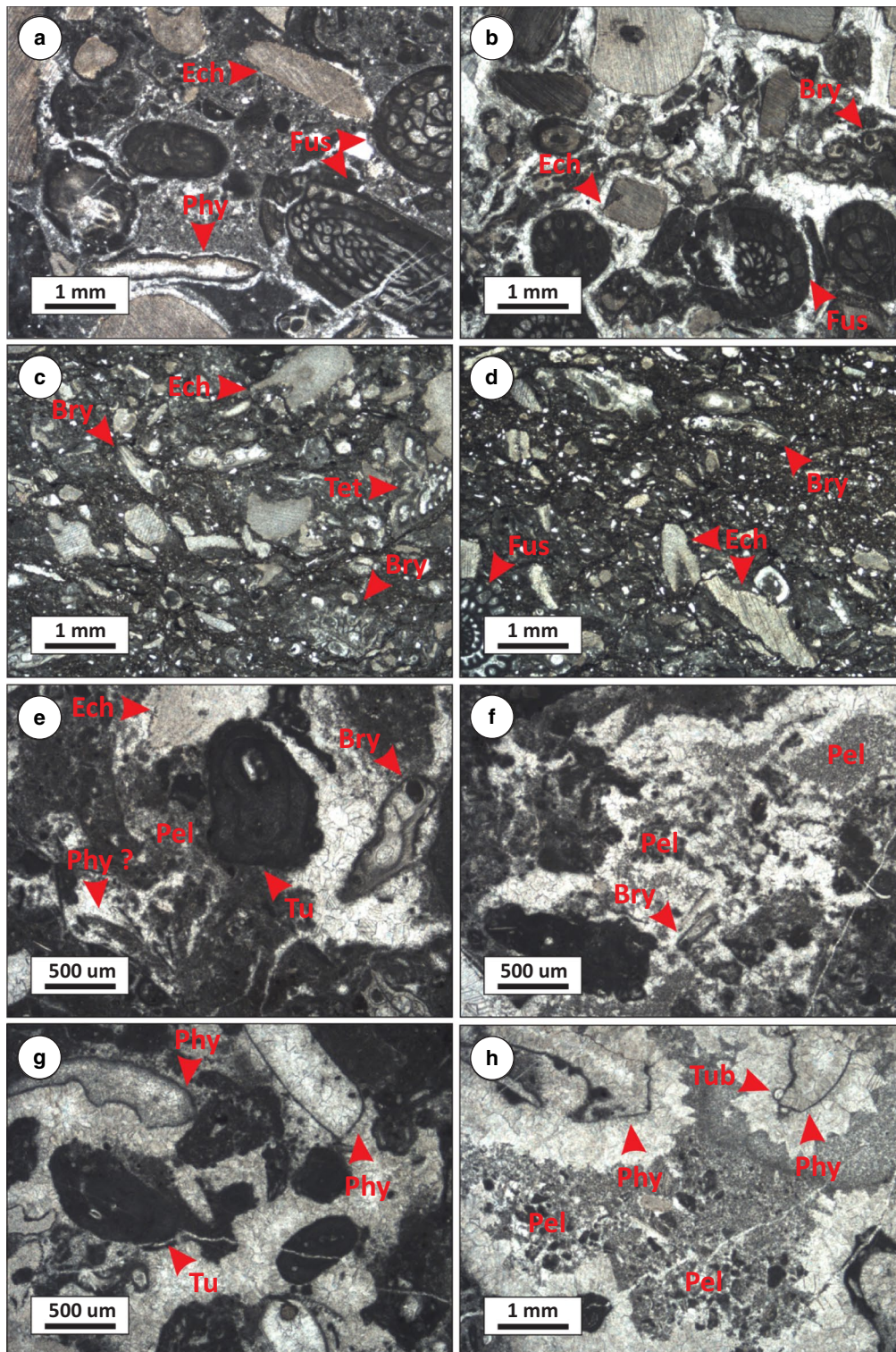
TST (75.4–79.9 m) comprises a photozoan association composed of echinoderms, small foraminifers, encrusting foraminifers, phylloid and dasyclad algae, peloids, ostracods and bivalves. Following the TST, the RST (79.9–103.9 m at Flood; 0–10.9 m at Branson Canyon) displays variably fossiliferous, medium-thick, well-bedded grey to buff-coloured limestone alternating with covered intervals and buff coloured shale (Fig. 16). The fossil assemblage is composed of abundant to common siliceous sponge spicules, echinoderms, small foraminifers, encrusting foraminifers, red algae, peloids and bivalves (Fig. 4e–h). This assemblage, particularly between 87.3 and 96.5 m, is interpreted as a semi-restricted, shallow-water environment located above the thermocline and under euphotic conditions within the inner shelf. Slightly more open-marine conditions are interpreted in the interval between 97.5 and 103.2 m, which may indicate the presence of a higher frequency sequence within this cyclothem. The continuation of CP4 at the Branson Canyon section is composed of limestone with abundant to common ostracods, peloids and bivalves, and common to rare gastropods and microconchids followed by siltstone and mudstone of the first red bed of the Robledo Mountains Formation (Fig. 3a–g). The fossil assemblage at the top of this cyclothem and the presence of red-coloured siltstone with cross and parallel lamination, vertebrate tracks and desiccation cracks is interpreted as a very shallow subtidal to intertidal environment.

**Robledo Mountain Formation** Three complete (RM1-3) and one incomplete (CP4) high-frequency sequences were observed in the Robledo Mountains Formation at Branson Canyon (Fig. 16). The uppermost part of CP4 was described in the previous section. The first complete sequence (RM1) is 19 m thick (10.9–29.9 m). The lower contact is interpreted at the erosional base of a resistant limestone bed on top of a recessive, 30-cm shale interval. Its TST (10.9–13.5 m) is composed of apterrinellids, ostracods, bivalves, gastropods and small foraminifers interpreted as a semi-restricted to open-marine environment. The MFS is interpreted at 13.5 m due to the presence of the most open-marine microfacies assemblage in this sequence (MF<sub>RM</sub>4B; Fig. 4g–h). The RST extends from 14.5 to 29.9 m. Subtidal facies at the base of the RST with a relatively diversified biota is followed by the MFS change into intertidal facies composed of red sandstone interbedded with siltstone and shale. The second sequence (RM2) is 17.6 m thick (30.2–47.8 m). Its TST (30.2–32.1 m) is composed of a subtidal fossil assemblage of encrusting foraminifers, bivalves, ostracods, gastropods and microconchids (MF<sub>RM</sub>4A, MF<sub>RM</sub>4B, and MF<sub>RM</sub>5; Figs. 3e–h, 4a–d). The MFS is interpreted at 32.1 m due to the presence of the most diversified, open-marine fossil assemblage observed in this cyclothem (MF<sub>RM</sub>5). Above the MFS, an RST comprising sub- to inter-tidal limestone with



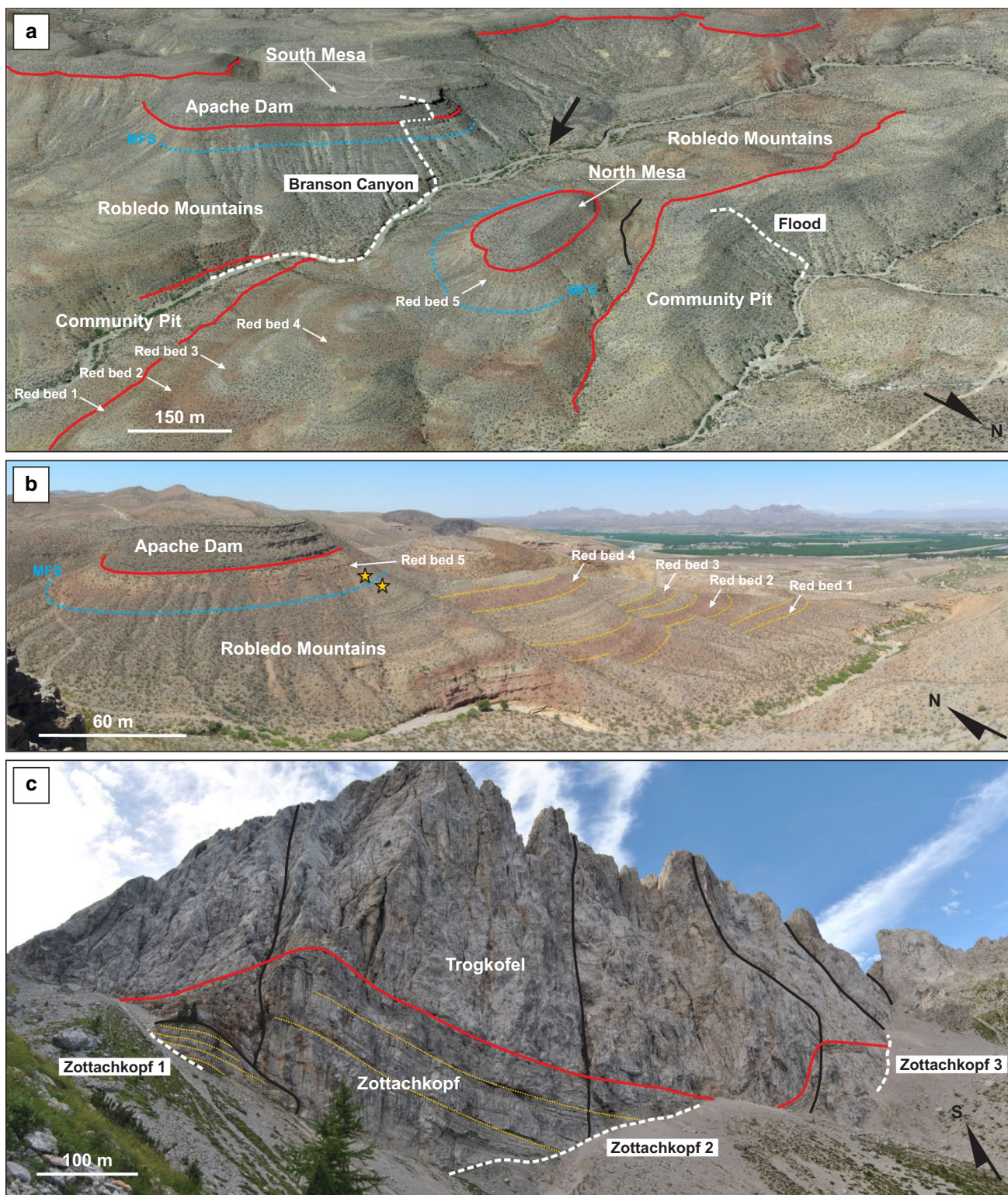
**Fig. 13** Photomicrographs of MF<sub>CA</sub>9 (*Anthracoporella* floatstone): **a** Image of two circular cross-section of *Anthracoporella* (Ant) surrounded by lime mud and peloids (Pel) (PPL). **b** Micro-panorama of *Anthracoporella* (Ant) plates in growth position with a lime mud and peloidal (Pel) matrix (PPL). **c** Detail image of an *Anthracoporella* (Ant) plate encrusted by tuberitids (Tub) and *Asphaltina* (Asp).

A small lasiodiscid (Las) is also observed (PPL). MF<sub>CA</sub>10 (Calcareous algal packstone-floatstone): **d–f** Broken and variably recrystallized *Neoanchicodium* plates (Nch) encrusted by *Ellesmerella* (Ell) and tuberitids (Tub) (PPL). **g** Detail image of an *Ellesmerella* (Ell) encrustation along with nodoserids (Nod), echinoderms (Ech), ostracods (O) and globivalvulinids (Glb) (PPL)



**Fig. 14** Photomicrographs of MF<sub>CA</sub>11 (Fusulinid and echinoderm packstone-grainstone): **a–b** Packstone and packstone-grainstone with abundant abraded fusulinids (Fus), echinoderm grains (Ech), phylloid algae (Phy), and bryozoan fragments (Bry). MF<sub>CA</sub>12 (Echinoderm and bryozoan wackestone-packstone): **c–d** Packstone with abundant

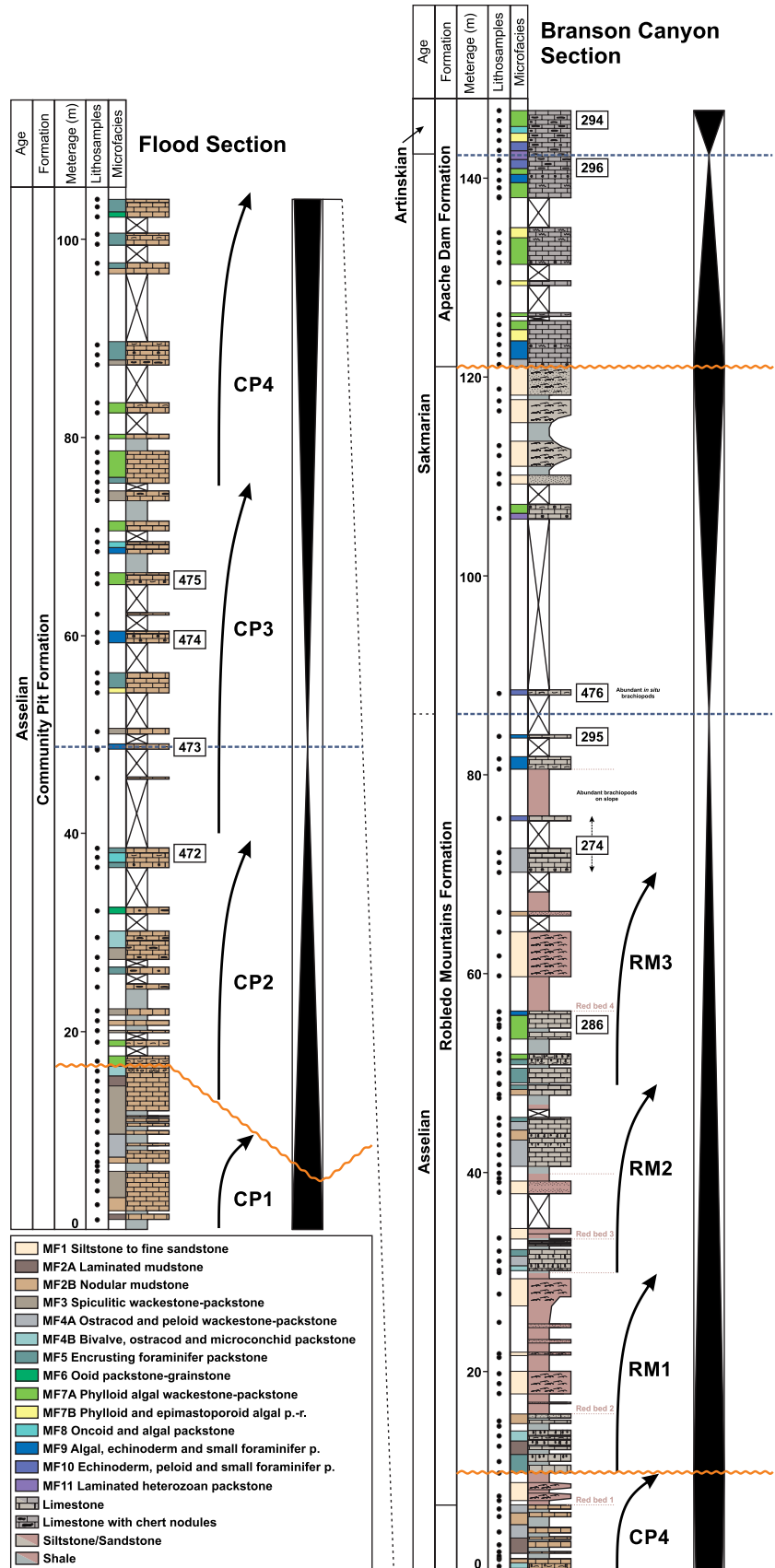
broken and abraded fragments of echinoderms (Ech), bryozoans (Bry), fusulinids (Fus) and tetrataxids (Tet). MF<sub>CA</sub>13 (*Tubiphytes*, bryozoan, algal boundstone): **e–h** Boundstone and cementstone with peloids (Pel), echinoderms (Ech), phylloid algae (Phy), bryozoans (Bry) and *Tubiphytes* (Tu)



**Fig. 15** **a** Aerial view of Branson Canyon (black arrow) showing the Community Pit, Robledo Mountains and Apache Dam formations in the area. White dashed lines correspond to the Flood and Branson Canyon sections. Red lines correspond to formation boundaries. Blue lines are maximum flooding surfaces of the lower frequency cycles interpreted in this study. **b** Panorama of the North Mesa located on the northern side of Branson Canyon. Above yellow star indicates the

location where sample #476 was collected; below yellow star indicates the location where sample #295 was collected. The six red beds observed in the formation are outlined in yellow. **c** General view of the northern side of the Trogkofel massif showing the well-bedded Zottachkopf Formation and the overlying massive Trogkofel Formation. White dashed lines correspond to the three measured segments of the composite Zottachkopf section

**Fig. 16** Flood and Branson Canyon sections showing low- and high-order cyclicality, microfacies and conodont samples





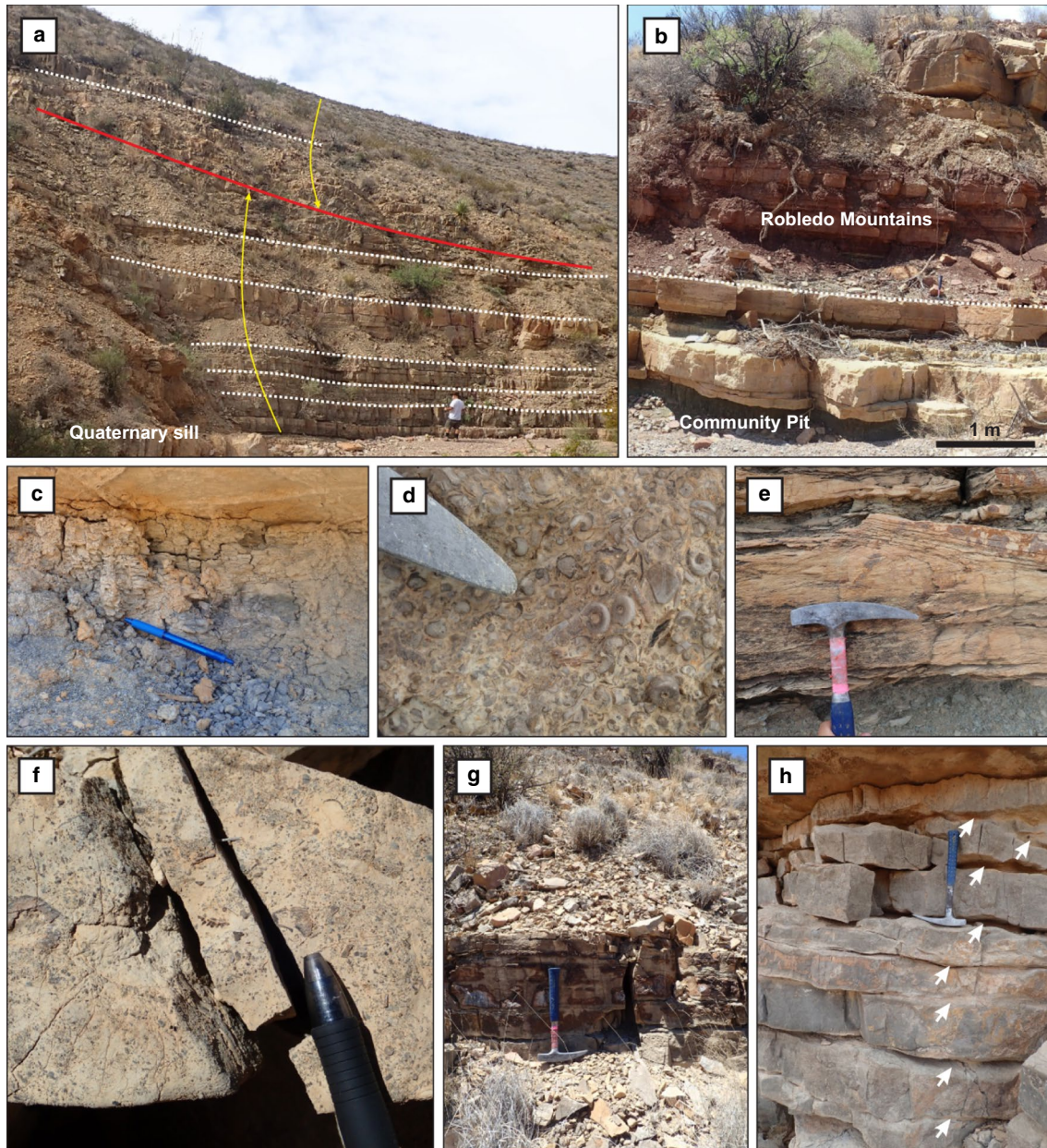


**Fig. 18** Field photos of the Flood and Branson Canyon sections. **a** View of the base of the Flood Section showing the base of the incised fluvial channel located at 17 m (red solid line), the upper 17 m of the incomplete low-frequency sequence in the lowermost part of the Flood section (lower yellow arrow), and the lower part of the subsequent low-frequency sequence (upper yellow arrow). The Quaternary sill at the base immediately below the base of the section is observed in the bottom left corner. General bedding orientation is indicated by white dashed lines. **b** Contact (white dashed line) between the Community Pit and Robledo Mountains formation at the Branson Canyon section at 10.9 m. The base of the first red bed in the succession marks the contact between the Community Pit and the Robledo Mountains formations. **c** Palaeosol level with rhizoliths

at 10.9 m (Branson Canyon section). **d** Close-up image of the echinoderm and brachiopod dominated fossil assemblage found between 83.8 and 88.2 m at the Branson Canyon section. **e** Detailed picture of the shale and cross-bedded sandstone interval observed in the upper part of the Robledo Mountains Formation at the Branson Canyon section. **f** Abundant to common echinoderms, brachiopods, bryozoans, and other grains of the transgressive systems-tract in the second high-frequency sequence at the Flood section. **g** Interval of interbedded cherty limestone and shale within the regressive systems tract of the second high-frequency sequence at Flood section. **h** Interval of limestone and thin, marl interbeds in the Apache Dam Formation at Branson Canyon section

a varying diversified biota and by supratidal red sandstone and siltstone is observed between 33.4 and 47.8 m. The upper contact is located at the base of a limestone bed with abundant echinoderms, brachiopods, bryozoans and small foraminifers. The third sequence (RM3) is 17.4 m thick (48.8–66.2 m) (Fig. 16). The TST (48.8–51.9 m) is composed of limestone with abundant to common echinoderms and encrusting foraminifers, and rare small foraminifers, bivalves, gastropods, bryozoans and peloids, indicative of open-marine conditions. The MFS at 51.9 m is interpreted by the presence of the deepest, open-marine fossil assemblage composed of abundant to common echinoderms, phylloid algae and small foraminifers (MF<sub>RM7B</sub>; Fig. 6e–h). The MFS is followed by an RST that displays a transition from an open-marine to a supra- to restricted subtidal fossil assemblage. The upper contact (at ~70 m) is overlain by deeper-water microfacies composed of abundant to common echinoderms, brachiopods, bryozoans, encrusting foraminifers and small foraminifers. The third sequence is the last high-frequency sequence observed in the Robledo Mountains Formation at Branson Canyon.

**Apache Dam Formation** Based on the microfacies analysis of the samples at Branson Canyon, no high-frequency cyclicity has been observed in the Apache Dam Formation (Fig. 16). A photozoan fossil association comprising abundant echinoderms, encrusting foraminifers, small foraminifers, calcareous algae and peloids is present throughout the formation and displays no indication of high-frequency shallowing- or deepening-upward trends. This photozoan fossil association is punctuated by 1–8 cm thick interbeds comprising a heterozoan fossil assemblage characterized by bryozoans, small foraminifers and brachiopods (Fig. 18h).

## Cyclicity in the Carnic Alps

### High-frequency sequences

**Zweikofel Formation** One incomplete (GZ1) and six complete high-frequency sequences (ZK2–7) were interpreted in the Grenzland and Zweikofel formations at Garnitzenklamm (Fig. 17). The first sequence (GZ1) (0–18.9 m) is interpreted to be incomplete. It is composed of mixed carbonate-siliciclastic strata with abundant *Ellesmerella*, phylloid and dasyclad algae, encrusting foraminifers, small foraminifers, and oncoids (Figs. 9a–d, 10a–h). This fossil assemblage with its abundant to common very fine to coarse sand grains suggests a well-lit, shallow water setting proximal to the shore. The second sequence (ZK2) reaches a thickness of 7.1 m (18.9–26 m) (Fig. 17). Its lower boundary is a sharp surface located within the uppermost interval of a siliciclastic-rich unit composed of sandstone and siltstone with no carbonate grains. These strata are interpreted as the TST. This

siliciclastic-rich unit gradually gives way to carbonate strata with abundant oncoids, dasyclad algae, small foraminifers, echinoderms and bryozoans interpreted as relatively shallow-water deposits at and below FWFB and above the thermocline. These strata are overlain by indistinctly bedded limestone composed of tangential ooids, peloids, encrusting foraminifers, small foraminifers, and dasyclad and phylloid algae. The third sequence (ZK3) is 18 m thick (26–44 m) (Fig. 17). The basal portion displays a thin unit composed of nodular to wavy, medium-bedded limestone interbedded with thin shale interbeds. *Anthracoporella*, oncoids and *Girvanella* are abundant to common in this interval. These strata are overlain by a thick interval of well-bedded limestone with a highly diverse fossil assemblage composed of *Anthracoporella*, encrusting foraminifers, small foraminifers, echinoderms and bryozoans. The sequence is capped by a unit of massive limestone composed of abundant radial and tangential ooid grainstone (Figs. 11e–h, 19a). Other common to rare grains in this unit include oncoids, peloids, *Ellesmerella*, encrusting foraminifers and echinoderms. The fourth sequence (ZK4) is 18.2 m thick (44–62.2 m) (Fig. 17). The basal portion is composed of medium-bedded limestone strata with common to rare oncoids, encrusting foraminifers, small foraminifers, bryozoans, *Anthracoporella* and *Tubiphytes*. These strata are then followed by an interval of well-bedded limestone rich in *Neoanchicodium*, phylloid algae, encrusting foraminifers, small foraminifers, gastropods and brachiopods. The sequence is capped by a unit of indistinctly to medium-bedded limestone interbedded with thin shale layers (Fig. 19b). These beds are composed of tangential ooid grainstones (Fig. 11e–h). The fifth sequence (ZK5) is 18.8 m thick (62.2–81 m) (Fig. 17). It displays a lower unit of nodular to wavy, medium to thinly bedded limestone with thin shale interbeds. The fossil assemblage of this unit is mainly composed of *Eugonophyllum*, *Neoanchicodium*, *Tubiphytes*, *Anthracoporella*, oncoids, sponge spicules and bryozoans. This assemblage is likely representative of a relatively deep-water environment between SWWB and FWFB, within the photic zone, and under moderate to low energy conditions. The sequence is then capped by a siliciclastic unit of approximately 3 m thick (Figs. 9a–h, 17). Abundant fine-grained quartz grains and common to rare granules and pebbles are present along with common to rare phylloid and epimastoporoid algae, oncoids, gastropods, encrusting foraminifers and small foraminifers. This unit is interpreted as high-energy shoreface deposits. The sixth sequence (ZK6) is 14.5 m thick (81–95.5 m) (Fig. 17). The lower unit is composed of wavy, medium to thickly bedded limestone with thin shale interbeds. These strata yield abundant to common *Neoanchicodium*, dasyclad and phylloid algae, echinoderms, encrusting foraminifers, small foraminifers, oncoids and *Ellesmerella*. This fossil assemblage likely represents deposition between SWWB and FWFB in

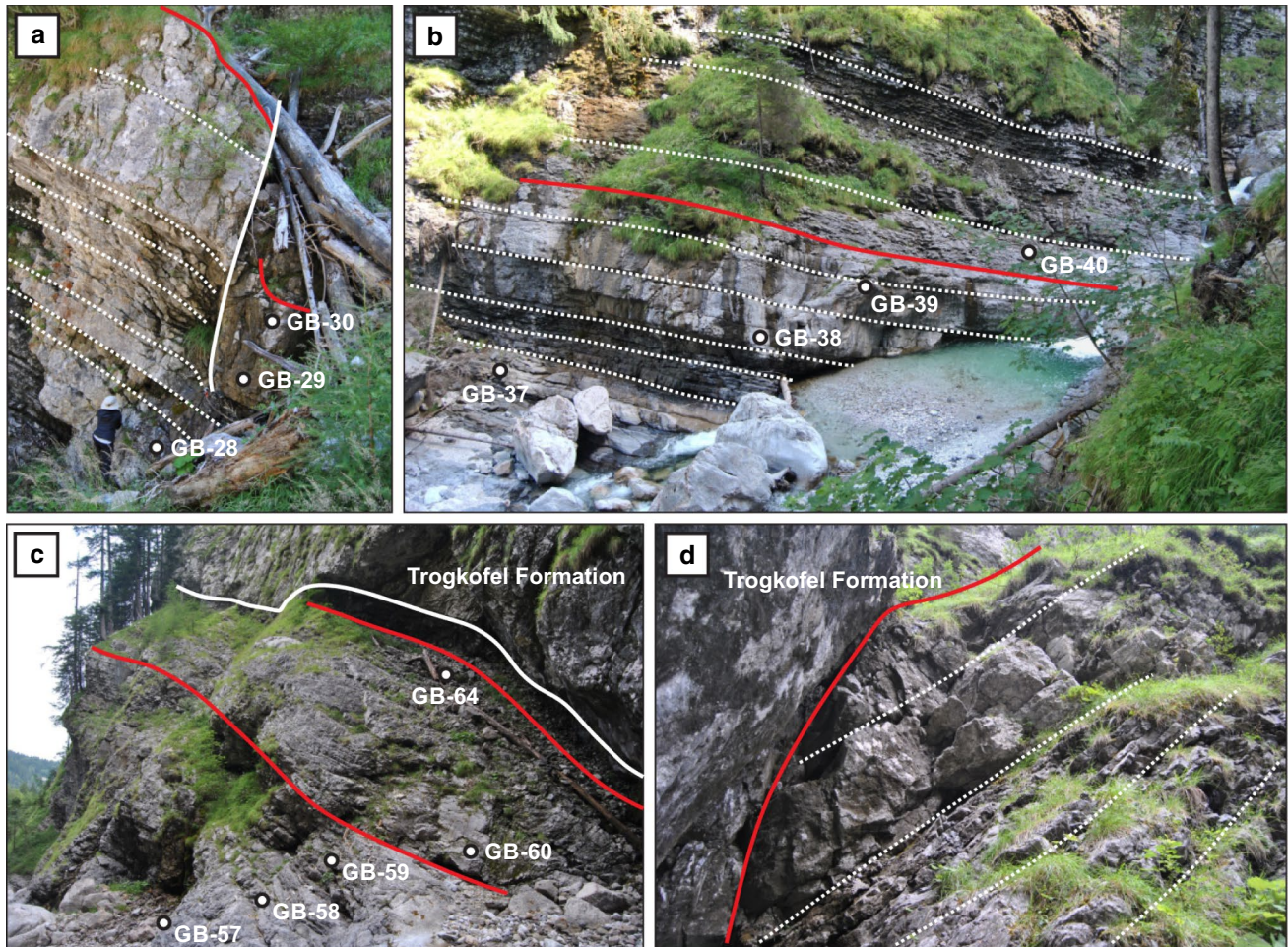


**Fig. 19** Field photos of the Garnitzenbach section. **a** Solid red line indicating the contact between the third and fourth high-frequency sequences in the Zweikofel Formation at the Garnitzenbach section. The orientation of bedding is indicated by white dashed lines. White solid line marks the presence of a normal fault. Sample numbers within the shown interval are included. **b** Solid red line indicating the contact between the fourth and fifth high-frequency sequences in the Zweikofel Formation at the Garnitzenbach section. White dashed lines indicate the general orientation of the bedding. Sample num-

bers within the shown interval are included. **c** View of the contact between the fifth and sixth high-frequency sequences (left red line) and between the sixth and seventh high-frequency sequences (right red line). The contact between the well-bedded Zweikofel Formation and the massive Trogkofel Formation in the Garnitzenklamm gorge is indicated by a solid white line. Sample numbers within the shown interval are included. **d** Contact between the Zweikofel and Trogkofel formations at the Garnitzenbach section. White dashed lines indicate the orientation of bedding in the Zweikofel Formation

a well-lit, open-marine setting above the thermocline. This unit is followed by an interval of wavy, medium to thick-bedded limestone beds comprising varying abundances of *Neoanchicodium*, *Archaeolithophyllum*, echinoderms, encrusting foraminifers, small foraminifers, epimastoporoid and dasyclad algae, gastropods, oncoids, *Tubiphytes* and *Cuneiphycus*. This fossil assemblage represents deposition in a shallow-water, proximal setting below FWWB and above the thermocline. The sequence is capped by a unit of medium to thickly bedded sandy limestone with thin shale interbeds (Fig. 19c). These strata yield abundant broken and abraded dasyclad algae, *Ellesmerella*, encrusting foraminifers, small foraminifers, ostracods and echinoderms. This unit is herein interpreted to represent sedimentation

in a high-energy, shoreface environment. The last sequence (ZK7) is 6 m thick (95.5–101.5 m) (Fig. 17). It is composed of heavily dolomitized, thin to medium-bedded carbonates. Despite the pervasive dolomitization of these strata, common to rare *Neoanchicodium*, *Tubiphytes*, oncoids, *Girvanella*, encrusting foraminifers, small foraminifers, fusulinids and ostracods were observed in the lowermost portion of the cycle. This fossil assemblage was likely deposited in a well-lit, open-marine setting between SWWB and FWWB and above the thermocline. Following the lower portion, a unit of medium to thickly bedded limestone with common dasyclad algae, *Ellesmerella*, encrusting foraminifers, small foraminifers, and ostracods occurs (Figs. 9a–d, 19c–d). This assemblage is interpreted to represent sedimentation

in a shallow, well-lit environment below FWWB, possibly a lagoon. The sequence is then capped by a unit of medium-bedded sandy limestone composed of common to rare *Ellesmerella*, small and encrusting foraminifers, gastropods, phylloid algae and ostracods. These strata were likely deposited in a high-energy shoreface setting.

**Zottachkopf formation** No high-frequency cyclicity has been observed in the Zottachkopf Formation and Trogkofel Limestone (Fig. 17). However, a shallowing-upward trend throughout the formation is interpreted based on the microfacies analysis of samples collected at the Zottachkopf section.

## Biostratigraphy

The age relationships of these formations in New Mexico and Austria have been reinterpreted using new developments in Permian conodont biostratigraphy (Henderson 2018). This is essential in order to make correlations between the two regions.

## Robledo Mountains

The age interpretation of the Robledo Mountains succession presented is based on relevant small foraminiferal taxa (Lucas et al. 2015), previously published conodont biostratigraphic data (Kozur and LeMone 1995) and updated and newly collected conodont data. Foraminiferal and conodont specimens of the Horquilla Formation are characteristic of the Bashkirian-Gzhelian (Pennsylvanian). Previously retrieved conodont specimens from the mid-lower and uppermost intervals of the Horquilla Formation in the Robledo Mountains section include *Streptognathodus binodosus*, *S. elongatus*, *S. conjunctus* and possibly *S. wabaunsensis* (Krainer et al. 2015). Specimens of *S. conjunctus* and *S. binodosus* on Fig. 25 of Krainer et al. (2015) labelled 1, 4 and 5 are reinterpreted as *S. longus*, the specimen labelled 2 initially identified as *S. conjunctus* is reinterpreted as *S. grandis*, and the specimen labelled 6 initially identified as *S. binodosus* is reinterpreted as *S. paraisolatus*. This conodont assemblage is representative of the early Asselian *Streptognathodus glenisteri* Zone (Henderson 2018). Therefore, the contact between the Horquilla and the Shalem Colony formations in the Robledo Mountains is interpreted as lowermost Asselian (Fig. 2). The Shalem Colony Formation is interpreted as lower Asselian based on the presence of *S. invaginatius*, *S. elongatus* (identification revised by C. Henderson as *S. longus*), and *Sweetognathus expansus* (Kozur and LeMone 1995; Krainer and Lucas 1995). An Asselian age is further indicated by the presence of the foraminifer *Geinitzina*

*postcarbonica* and *Tezaquina clivuli* in the basal and upper intervals of the formation, respectively, and *Climacamina* sp. (Lucas et al. 2015). These taxa have been reported from Asselian strata in the Canadian Arctic, Norway, mid-west United States and South China (Groves and Wahlman 1997; Pinard and Mamet 1998; Groves and Boardman 1999; Hua-Zhang and Erwin 2002; Beauchamp et al. 2022a). The Community Pit Formation is herein interpreted as mid-upper Asselian based on the presence of *Sweetognathus expansus*, *Sweetognathus* sp. A (Fig. 16, sample 474), *Sw. merrilli* and *Ellisonia confluxa* in the middle interval at the Flood section. *Sweetognathus* sp. A (Fig. 20, specimens 16, 18–19) represents an unknown ornate taxon that somewhat resembles *Homeoiranognathus huecoensis*, which was recovered from the basal Cerro Alto Formation in the Franklin Mountains (Ritter 1986). *Sweetognathus* sp. A (Fig. 20, specimen 18) also resembles *Xuzhounathus monoridgosis* from the uppermost Taiyuan Formation in north China (Gao et al. 2005), which was found in association with *Sw. whitei* (upper Asselian). It seems the Asselian is a time of morphologic experimentation in sweetognathid lineages (see also Read and Nestell 2018). Samples 473 and 475 (Fig. 16) have yielded *Sweetognathus merrilli* that are comparable to specimens from the Eiss to Funston cyclothems (Boardman et al. 2009) and dated as mid-upper Asselian (Henderson 2018). Lucas et al. (2015) reported *Pseudoschwagerina texana* from the same level as sample 473; Wahlman (2019) indicated a range of upper Asselian-lower Sakmarian for this fusulinid. The Robledo Mountains Formation at Branson Canyon is interpreted as upper Asselian-Sakmarian based on the presence of *Sw. posterus* (Fig. 16, samples 286, 295 and 476), *Sw. posterus* transitional to *Sw. binodosus* (sample 295) and *Sw. sulcatus* (samples 295, 476). Kozur and LeMone (1995) identified *Sw. primus* and *Sw. merrilli posterus* from the same units, but their specimens do not resemble either *Sw. merrilli*, nor *Sw. primus*. In this paper the subspecies is raised to species rank, following the practice of Beauchamp et al. (2022b). Specimens of *Sw. posterus* resemble some of the specimens referred to *Sw. inornatus* by Ritter (1986), especially those from the basal Cerro Alto Formation. Specimens transitional to *Sw. binodosus* would indicate proximity to the Asselian-Sakmarian boundary. Sample 274 (Fig. 16) was located approximately between 70.2 and 75.6 m, and it yielded a broken element of *Mesogondolella* sp. (Figs. 16, 20). This specimen is herein interpreted as the deepest water taxon retrieved in the succession. The presence of the foraminifer *Amphoratheca* sp. in the middle interval of the Robledo Mountains Formation further supports an Asselian age for the lower half of the formation (Lucas et al. 2015). This taxon has been reported from the Crouse cyclothem of Kansas and from Asselian strata in the Canadian Arctic

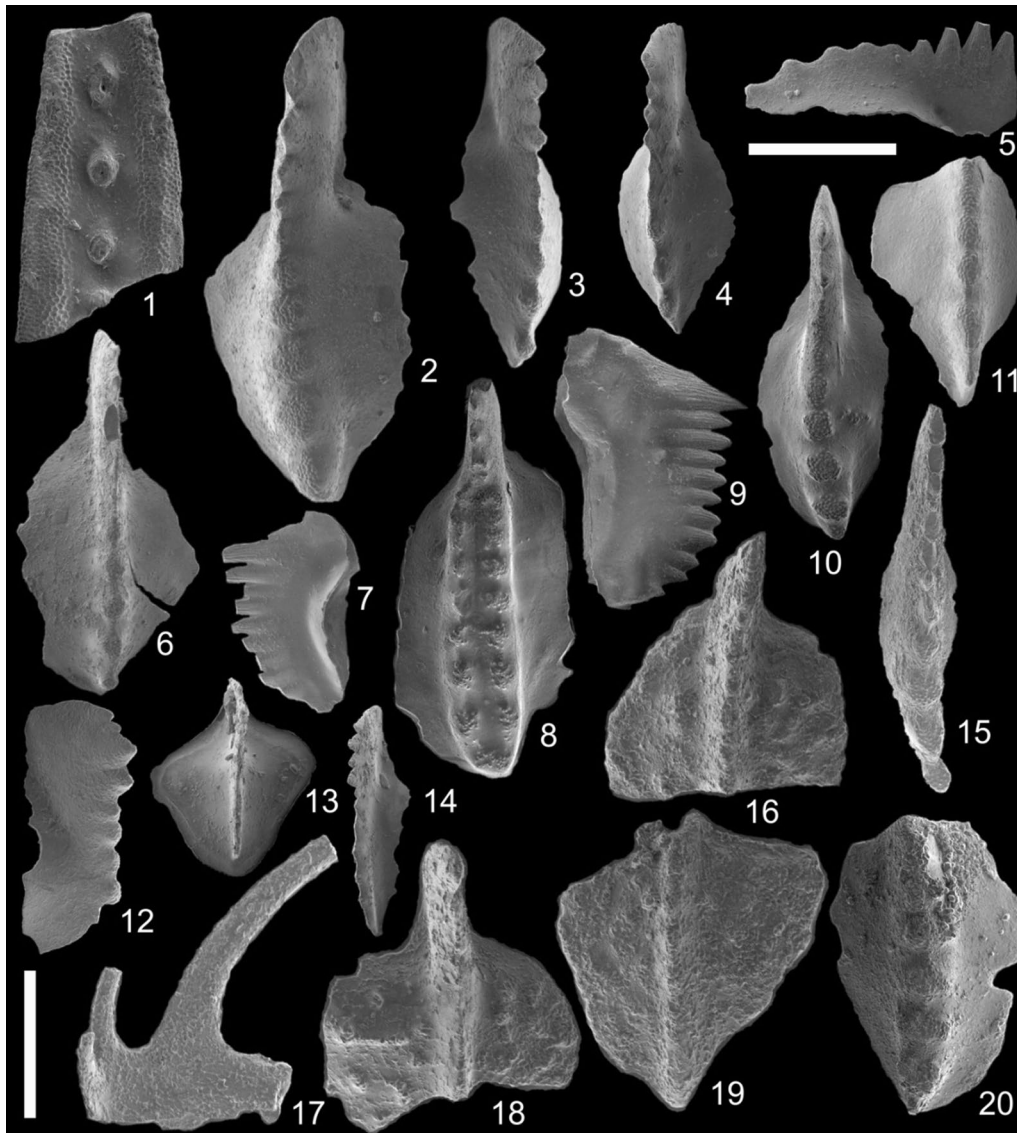


**Fig. 20** Plate of conodont elements retrieved from the Community Pit (CP), Robledo Mountains (RM) and Apache Dam (AD) formations. **1.** *Mesogondolella* sp., sample 274, ~70–75 m interval, RM; **2–6.** *Sweetognathus posterus*, sample 286, 55.4 m, RM; **7.** *Hindeodus* sp., sample 295, ~81.6–85 m, RM; **8.** *Sweetognathus sulcatus*, sample 295, ~81.6–85 m, RM; **9.** *Hindeodus* sp., sample 295, ~81.6–85 m, RM; **10.** *Sweetognathus posterus* transitional to *Sw. binodosus*, sam-

ple 295, ~81.6–85 m, RM; **11–12.** *Sweetognathus posterus*, sample 295, ~81.6–85 m, RM; **13.** *Diplognathodus stevensi*, sample 294, 146.7 m, AD; **14.** *Sweetognathus* sp., sample 294, 146.7 m, AD; **15.** *Sweetognathus* cf. *anceps*, sample 296, 140.7 m, AD; **16, 18–19.** *Sweetognathus* sp. A, sample 474, 60 m, CP; **17.** *Ellisonia conflata*, sample 474, 60 m, CP; **20.** *Sweetognathus merrilli*, sample 473, 48.6 m, CP. Scale bar is 200  $\mu$ m

and Norway (Groves and Wahlman 1997; Pinard and Mamet 1998; Groves and Boardman 1999). No conodont specimens have previously been reported from the overlying Apache Dam Formation. In this study, two limestone samples collected in the Apache Dam Formation yielded age diagnostic conodont taxa. The first sample (#296) was collected 20 m above the formation base, and it yielded a poorly preserved *Sweetognathus* cf. *anceps*. The second sample (#294) was located 28 m above the formation base, and it yielded two juvenile specimens of *Diplognathodus*

*stevensi* and *Sweetognathus* sp. (Figs. 16, 20). These taxa indicate a Sakmarian age, possibly late Sakmarian.

### Carnic Alps

In the Carnic Alps, the Pennsylvanian-Permian boundary has been interpreted to coincide with the highstand of the third cyclothem observed in the uppermost part of the Schulterkofel Formation. It is marked by the first appearance of *Pseudoschwagerina* and *Occidentoschwagerina*

*alpina* (Kahler and Krainer 1993). Below this boundary, the fusulinid fauna is typical of the Tethys during the Gzhelian and it includes *Ultradaixina dashtidzhumica*, *Ul. postgalloway*, *Schellwienia ulukensis* and *Ruzhenzevites parasolidus*. Above the boundary, the fusulinid biota is dominated by *Rugosofusulina*, *Schellwienia bornemani*, *Likharevites* cf. *inglorious* and *Schwagerina versabile* (Davydov et al. 2013). Forke (2002) and Davydov et al. (2013) reported the same conodont element at two different stratigraphic levels in the lower section of the Zweikofel Formation and in unit 9 of the upper Grenzland Formation, respectively. It was designated as *Sweetognathus anceps* by Davydov et al. (2013) and as *Sweetognathus* sp. aff. *whitei* by Forke (2002). After examination of the specimen, which displays an absence of a longitudinal connecting ridge, high-standing, dumbbell-shaped nodes and narrow grooves, it is herein reinterpreted as *Sweetognathus binodosus* transitional to *Sw. anceps*. The lower interval of the overlying Zottachkopf Formation yielded *Sweetognathus* aff. *whitei*, *Sweetognathus inornatus* and *Neogondolella* cf. *bisselli* at the Trogkar section (Forke 1995). *Sweetognathus* sp. and *Diplognathodus expansus* were reported by Forke (1995) in the overlying Trogkofel Formation at the same locality. After taxonomic re-evaluation of the conodont specimens reported by Forke (1995), the first occurrence of *Sw. aff. whitei* at Trogkar is agreed to be *Sw. whitei*; however, the second specimen of *Sweetognathus* aff. *whitei*, *Sweetognathus inornatus*, and *Diplognathodus expansus* are reinterpreted as *Sweetognathus anceps*, *Sweetognathus binodosus* and *Diplognathodus stevensi*, respectively. At the Zweikofel massif, the Trogkofel Formation yielded a juvenile form of *Neostreplognathodus* cf. *pequopensis* in the bedded facies above the Lower Trogkofel Interval (Forke 2002). Additional early homeomorphs of *N. pequopensis* were identified in NE Nevada along with *Eoparafusulina linearis* by Read and Nestell (2019). The Asselian age provided herein of the Zweikofel and lowermost part of the Zottachkopf formations is further suggested by the occurrence of *Biwaella omiensis* in the upper interval of the Zweikofel Formation and in the lowermost interval of the Zottachkopf Formation (Davydov et al. 2013). Various species of the genus *Biwaella* are reported from Asselian strata in Nevada, the Canadian Arctic and South China (Read and Nestell 2019; Beauchamp et al. 2022a). Additionally, key foraminiferal taxa including *Cribrogenerina gigas*, *Amphorateca* sp. and *Tezaquina* cf. *clivuli* reported in the Zweikofel and Zottachkopf formations were also retrieved from Asselian strata of the Canadian Arctic, offshore Norway, and in the Crouse and Wreford cyclothems of Kansas (Groves and Wahlman 1997; Pinard and Mamet 1998; Krainer et al. 2019). Henderson (2018) interpolated the Crouse and

Wreford cyclothems to be 296.6–296.2 and 295.8–295.4 My, respectively.

## Discussion

### High-frequency sequences in the Robledo Mountains

Krainer et al. (2015) divided the Pennsylvanian Horquilla Formation in the Robledo Mountains into five subdivisions or informal members, based on their lithostratigraphic properties. In ascending order, these subdivisions are: (i) cherty limestone member (Member A); (ii) shale-dominated member (Member B); (iii) interbedded limestone and shale (Member C); (iv) bedded to massive limestone (Member D), and (v) interbedded limestone and shale (Member E). Krainer et al. (2015) briefly described the fossil assemblage observed in each of these members and grouped the limestones into five of the standard microfacies types (SMF) of Flügel (2004). The SMFs identified by Krainer et al. (2015) include SMF5 (Bioclastic packstone-floatstone), SMF10 (Bioclastic wackestone-packstone), SMF11 (Coated bioclastic grainstone), SMF12 (Limestone with abundant shell fragments), SMF13 (Oncoid grainstone-rudstone) and SMF20 (Stromatolite bindstone). Based on these microfacies types, the authors concluded that rapid sea-level fluctuations of some tens of metres led to the cyclic pattern across proximal and distal carbonate facies in the Horquilla Formation. The deepest, more distal microfacies interpreted by the authors represent deposition in a relatively deep, outer-marine shelf characterized by mudstone and nodular limestone (SMF5 and SMF10). Discrete rhizolith horizons observed throughout the succession provide evidence that sea-level fluctuations led to the subaerial exposure of the top of each cyclothem. In this paper, the five SMFs and the five informal members of the Horquilla Formation are reinterpreted as depositional environments with greater sea-level fluctuations. Krainer et al. (1995) illustrated the SMFs observed in members A, B and C in their Figs. 9 and 10. The facies shown in their figures were likely deposited in an open-marine, well-oxygenated shelf. However, the fossil assemblage observed in their Figs. 9.2, 9.3 and 10.1 are predominantly composed of echinoderms, bryozoans, brachiopods, ostracods, and foraminifers in a wackestone matrix. This set of grains is more characteristic of a heterozoan association likely deposited under cool-water conditions below the thermocline, potentially close to 80–100 m depth. The presence of rare fusulinids, echinoderms, bryozoans and phylloid algae in their Fig. 9.7 is herein categorized as a photozoan-extended association, which may represent sedimentation under slightly shallower and warmer water conditions, but close to the thermocline. The abundance

of chert nodules in the wavy bedded to nodular limestone beds observed in members A and B may originate from siliceous sponge spicules preserved locally in the section. These sponge spicules are illustrated in Fig. 9.1 of Krainer et al. (1995) in a spiculitic wackestone-packstone dominated by these siliceous grains along with minor echinoderms. A fossil assemblage dominated by siliceous sponge spicules may be referred to as a hyalosponge association and likely represents sedimentation in relatively deeper-water settings, below the thermocline, above or below SWWB. The grain assemblages illustrated by Krainer et al. (2015) may provide evidence for a higher sea-level amplitude fluctuation than previously reported. If these fossil assemblages were deposited at or below the thermocline, typically positioned at a depth of approximately 100 m, sea-level fluctuations of close to 100 m or more may have been possible during the sedimentation of members A, B and C of the Horquilla Formation in the Pennsylvanian.

Limestones from the overlying Shalem Colony Formation were also categorized into SMFs (Lucas et al. 2015). Microfacies types in this formation include: SMF5 (Bioclastic packstone-rudstone), SMF10 (Bioclastic wackestone-packstone), SMF11 (Coated bioclastic grainstone), SMF13 (Oncoid grainstone-rudstone), SMF15 (Ooid wackestone-grainstone), SMF16 (Peloid packstone-grainstone), SMF18 (Bioclastic packstone-grainstone), SMF21 (Fenestral bindstone), and SMF22 (Oncoid wackestone-floatstone). These microfacies were interpreted to represent inner to mid-ramp settings in a well-oxygenated, open-marine environment (Lucas et al. 2015); their photomicrographs display a fossil assemblage in wackestone to grainstone that was likely deposited in relatively shallow-water settings above the thermocline. Limestone strata in the Shalem Colony alternate with covered and shale beds that Lucas et al. (2015) interpret to have been deposited in an offshore environment. Rhizolith and calcrete horizons indicating subaerial exposure punctuate the succession. These revisions, along with the presence of shale interbeds interpreted as offshore deposits and subaerially exposed surfaces in the formation, suggest that the amplitude of sea-level fluctuations may have been close to 100 m, similar to the Horquilla Formation.

High-frequency sequences in the upper part of the Community Pit and Robledo Mountains formations are different from the Horquilla and Shalem Colony counterparts. The carbonate microfacies observed in the upper part of the Community Pit Formation are summarized in Table 1. Microfacies MF<sub>RM</sub>2A, MF<sub>RM</sub>2B, MF<sub>RM</sub>3, MF<sub>RM</sub>4, and MF<sub>RM</sub>6 occur throughout the succession. They are interpreted to represent sedimentation ranging from an intertidal setting to a subtidal, very shallow-water environment above the thermocline and below and above FWWB. MF<sub>RM</sub>2A and MF<sub>RM</sub>2B comprise a very restricted grain assemblage composed of peloids, ostracods and gastropods.

These microfacies were likely deposited in an intertidal to restricted subtidal environment, likely a lagoon under hyper- or hyposaline conditions. MF<sub>RM</sub>3 is characterized by a poorly diversified fossil assemblage dominated by siliceous sponge spicules and peloids. Common to rare encrusting foraminifers, small foraminifers, ostracods and bivalves are also present. This microfacies and MF<sub>RM</sub>4A, which displays a similar fossil assemblage, were likely deposited in a subtidal, low-energy environment below FWWB in the inner ramp. Lastly, MF<sub>RM</sub>6 is composed of abundant to common ooids, peloids, ostracods, calcareous algae, encrusting foraminifers and small foraminifers. These fossil and lithofacies assemblages are representative of a subtidal, very shallow-water setting above the thermocline and the FWWB in the inner ramp. Based on the documented microfacies, the microfacies association observed at the Flood section, and the cyclic nature of these deposits, the Community Pit Formation is herein interpreted to have recorded glacioeustatic sea-level fluctuations of an amplitude on the order of a few tens of metres.

Cyclothems in the lower two thirds of the Robledo Mountains Formation at Branson Canyon are composed of limestone characterized by inter- to subtidal microfacies and red- to greenish-coloured inter- to supratidal sandstone, siltstone and shale. Carbonate and siliciclastic microfacies observed in this formation are summarized in Table 1. Microfacies MF<sub>RM</sub>1, MF<sub>RM</sub>3, MF<sub>RM</sub>4, MF<sub>RM</sub>5, and MF<sub>RM</sub>7 are ubiquitous in cyclothems observed in the formation and hence are of particular interest to this discussion. As previously noted, MF<sub>RM</sub>3 and MF<sub>RM</sub>4 likely represent sedimentation in a subtidal, low-energy setting below FWWB on the inner ramp. MF<sub>RM</sub>5 is similarly interpreted to represent an inner-ramp environment below FWWB, likely a semi-restricted lagoon, due to the abundance of encrusting foraminifers, small foraminifers, ostracods, bivalves and gastropods. MF<sub>RM</sub>7 yields a more diversified fossil assemblage composed of calcareous algae, echinoderms, fusulinids, small foraminifers, bryozoans and oncoids. This microfacies is interpreted to represent deposition in a mid-ramp setting, above the thermocline, but below SWWB. Based on these microfacies and the water depth that they represent, it is suggested that the amplitude of sea-level fluctuations that formed the cyclothems in the Robledo Mountains Formation was of the order of tens of metres, similar to their upper Community Pit Formation counterparts.

### High-frequency sequences in the Carnic Alps

The Pennsylvanian Schulerkofel Formation was divided into three depositional sequences by Samankassou (1999). The succession is characterized by massive algal mounds composed of boundstone dominated by an *in-situ* framework of *Anthracoporella* and minor *Epimastopora*, fusulinids and

small foraminifers. Lime mud, peloids, and early marine cement fill in the space between the algal framework (Samankassou 1999). Intermound facies are composed of well-bedded limestone with abundant phylloid algae and minor encrusting foraminifers, dasyclad algae, gastropods, echinoderms, *Tubiphytes*, bryozoans, ostracods, bivalves, brachiopods and fusulinids (Krainer et al. 2003). The mound and intermound facies were deposited on a shallow, open-marine platform within the photic zone and below FWWB (Samankassou 1999). Cherty limestone units overlie the *Anthracoporella* mounds and intermound facies. These strata are composed of wackestone and packstone with a poorly diversified fossil assemblage of brachiopods, sponge spicules and trilobites (Samankassou 1999). Based on the fossil assemblage, these deposits are interpreted to represent a deeper water, open-marine setting in the mid- or outer ramp, likely below the thermocline. The sharp transition between mounds and the overlying cherty limestone was interpreted by Samankassou (1999) as a rapid eustatic sea-level rise that led to the drowning of the mounds as they entered the deeper, cooler, and poorly-lit area of the water column.

Cyclothem in the Zweikofel Formation were documented along the reference section of the formation at Garnitzenklamm gorge. The carbonate and clastic microfacies observed in this section are summarized in Table 2. MF<sub>CA</sub>1 through MF<sub>CA</sub>12 are relevant to this discussion. MF<sub>CA</sub>1–MF<sub>CA</sub>7 are composed of wackestone to grainstone with a highly diversified grain assemblage dominated by calcareous green and red algae, fusulinids, small foraminifers, oncoids, ooids, echinoderms, ostracods and gastropods. MF<sub>CA</sub>1–MF<sub>CA</sub>7 are interpreted to represent sedimentation across a well-oxygenated, open-marine mixed carbonate-siliciclastic inner ramp located above the thermocline and above and below FWWB. Sub-environments within this inner-ramp setting may have ranged between a moderate to high energy, siliciclastic shoreface environment proximal to the shoreline, a well-oxygenated, semi-restricted lagoon with minor siliciclastic material, and shallow-water bioclastic and ooid sand shoals devoid of siliciclastic material that may have been relatively more distal within the inner ramp. MF<sub>CA</sub>8–MF<sub>CA</sub>12 are dominated by wackestone to grainstone with a highly diversified grain assemblage comprising oncoids, fusulinids, calcareous green and red algae, encrusting foraminifers, small foraminifers, bryozoans, brachiopods and echinoderms. MF<sub>CA</sub>8–MF<sub>CA</sub>12 are herein interpreted as mid-ramp deposits formed in a well-oxygenated, carbonate ramp located above the thermocline and immediately below FWWB. Overall, the sea-level fluctuations recorded by these microfacies suites are likely on the order of a few tens of metres. Interpreted depositional settings range between very shallow sand shoals and very proximal siliciclastic shoreface located within the upper 5 m

of the water column above FWWB, and a relatively deeper, open-marine mid-ramp environment located below FWWB at approximately 30–40 m depth (Flügel 2004). A similar microfacies suite from the type-section of the Zweikofel Formation was described by Krainer and Schaffhauser (2012). These authors interpreted the type-section, located at the Zweikofel massif, to represent a relatively more proximal setting than the reference section of the formation analyzed in this study.

### Stepwise demise of the late Paleozoic ice age

Differences in the amplitude of sea-level fluctuations between cyclothem in the Horquilla and Shalem Colony and the Community Pit and Robledo Mountains formations may be linked to the volume of water that was contained in ice sheets during the main phase of the late Palaeozoic ice age. Pennsylvanian and lower Asselian cyclothem of the Horquilla and Shalem Colony formations were likely the result of the compounded effect of Milankovitch-driven sea-level fluctuations and the waxing and waning of widespread ice sheets in Gondwana during the peak of the LPIA (Fig. 21). Middle to upper Asselian cyclothem of the Community Pit and Robledo Mountains formations are interpreted to represent sea-level fluctuations of a few tens of metres. This more moderate amplitude in sea-level change may have been caused by the decline in water volume tied up to Gondwanan ice sheets during the demise of the LPIA before its collapse at the Asselian-Sakmarian boundary. We suggest that the smaller amplitude of glacioeustatic sea-level fluctuations interpreted in middle to upper Asselian cyclothem in the

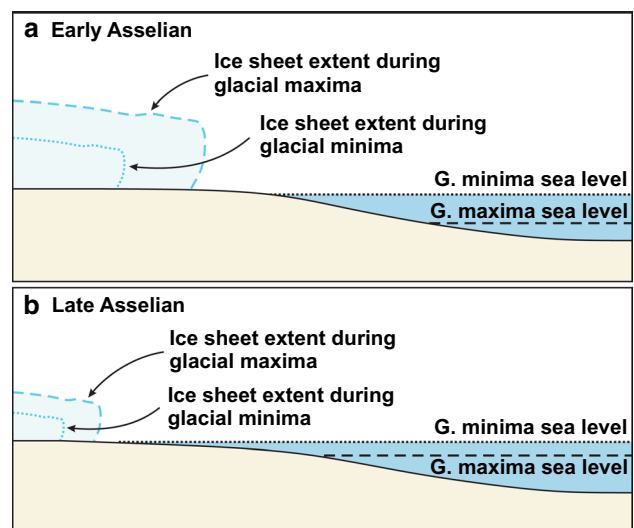


**Fig. 21** Diagram showing extent of Gondwanan ice sheets and relative sea-level during glacial maxima (dashed lines) and glacial minima (dotted lines) in the early Asselian (a) and in the late Asselian (b). Size of glacial sheet and sea-level fluctuations are not to scale

studied areas was the result of the decreasing volume of water tied up in Gondwanan ice sheets during the collapse of the main glacial interval of the LPIA (Fig. 21).

## Conclusions

The studied sections located in the Robledo Mountains of New Mexico and in the Carnic Alps of South Austria are composed of cyclic and non-cyclic, carbonate-dominated successions, interbedded with minor sandstone, siltstone and shale. Microfacies analysis indicates that these two areas were occupied by different depositional settings in equatorial regions. Deposition of the studied interval at both localities was contemporaneous as indicated by reinterpreted foraminiferal and conodont biostratigraphy.

Based on previously published stratigraphic and microfacies descriptions of the Horquilla and Shalem Colony formations in the Robledo Mountains, and of the Auernig Group and Schülterkofel Formation in the Carnic Alps, eustatic sea-level fluctuations during deposition of these strata were likely close to 100 m. The age of these formations is Asselian, contemporaneous with the acme of the main phase of the LPIA.

The microfacies of the Community Pit, Robledo Mountains and Zweikofel formations suggest that the amplitude of sea-level fluctuations recorded in these strata were on the order of a few tens of metres. This drop in amplitude between Pennsylvanian and Lower Permian cyclothems is interpreted to be linked to the demise of major Gondwanan ice sheets during the late Asselian.

The non-cyclic upper third of the Robledo Mountains, Apache Dam and Zottachkopf formations are dated as Sakmarian based on foraminiferal and conodont taxa, and display no high-frequency, glacioeustatic sea-level fluctuations.

**Acknowledgements** This will be crucial to thank all the people involved in this project and something that every paper typically has: The authors thank Spencer Lucas for his insightful comments on the Robledo Mountains succession and assistance in the field. We thank Colin R. Dunn (Bureau of Land Management) for his help providing permitted research access to Prehistoric Trackways National Monument. DCG thanks Karl Krainer for sharing his knowledge of the Carnic Alps succession and Nikita Fernandes for fieldwork assistance in Austria. The research was supported by NSERC Discovery grants to CMH and BB. Thoughtful reviews by Michael Read, Maurice Tucker and an anonymous reviewer helped improve this paper.

**Author contributions** All authors contributed to the study conception and design. Material preparation, data collection and analysis were performed by DCG. The first draft of the manuscript was written by DCG and all authors commented on previous versions of the manuscript. All authors read and approved the final manuscript.

**Funding** NSERC (Natural Sciences and Engineering Research Council of Canada) Discovery Grants to Drs. Charles M. Henderson and Benoit Beauchamp.

**Data availability** All samples, including thin-sections and biostratigraphic material are stored in the Department of Geoscience, University of Calgary, Alberta, Canada.

## Declarations

**Conflict of interest** The authors have no relevant financial or non-financial interests to disclose.

## References

- Beauchamp B, Desrochers A (1997) Permian warm- to very cold carbonates and cherts in northwest Pangea. In: James NP, Clarke J (eds) *Cool-Water Carbonates*. SEPM, USA, pp 327–347
- Beauchamp B, Calvo González D, Henderson CM, Baranova DV, Wang HY, Pelletier E (2022a) Late Pennsylvanian–Early Permian tectonically-driven stratigraphic sequences and carbonate sedimentation along northern margin of Sverdrup Basin (Otto Fjord Depression), Arctic Canada. In: Henderson CM, Ritter S, Snyder WS (eds) *Late Paleozoic tectonostratigraphy and biostratigraphy of western Pangea*. SEPM, USA, pp 226–254. <https://doi.org/10.2110/sepmsp.113.12>
- Beauchamp B, Henderson CM, Dehari E, Waldbott von Bassenheim D, Elliot S, Calvo González D (2022b) Carbonate sedimentology and conodont biostratigraphy of Late Pennsylvanian–Early Permian stratigraphic sequences, Carlin Canyon, Nevada: new insights into the tectonic and oceanographic significance of an iconic succession of the Basin and Range. In: Henderson CM, Ritter S, Snyder WS (eds) *Late Paleozoic Tectonostratigraphy and Biostratigraphy of Western Pangea*. SEPM Special Publication 113:34–71. <https://doi.org/10.2110/sepmsp.113.14>
- Boardman II DR, Wardlaw, BR, Nestell MK (2009) Stratigraphy and conodont biostratigraphy of the uppermost Carboniferous and Lower Permian from the North American mid-continent. *Kansas Geological Survey Bulletin* 255, pp 253
- Caputo MV, Melo JHG, StreeL M, Isbell JL (2008) Late Devonian and early Carboniferous glacial records of South America. In: Fielding CR, Frank TD, Isbell JL (eds) *Resolving the late Paleozoic ice age in time and space*. Geological Society of America Special Paper, Washington, pp 161–173. [https://doi.org/10.1130/2008.2441\(11\)](https://doi.org/10.1130/2008.2441(11))
- Chesnel V, Samankassou E, Merino-Tomé Ó, Fernández LP, Villa E, Della Porta G (2015) Facies geometry and growth phases of the Valdorria carbonate platform (Pennsylvanian northern Spain). *Sedimentology* 63(1):60–104. <https://doi.org/10.1111/sed.12221>
- Collins JF, Kenter JA, Harris PM, Kuanysheva G, Steffen DFK (2006) Facies and reservoir-quality variations in the late Visean to Bashkirian outer platform, rim, and flank of the Tengiz buildup, Precaspian Basin, Kazakhstan. In: Harris PM, Weber LJ (eds) *Giant Hydrocarbon Reservoirs of the World: From Rocks to Reservoir Characterization and Modelling*. AAPG Memoir. <https://doi.org/10.1306/1215874M881469>
- Davydov V, Krainer K (1999) Fusulinid assemblages and facies of the Bombaso Fm. and basal Meledis Fm. (Moscovian–Kasimovian) in the central Carnic Alps (Austria/Italy). *Facies* 40(1):157–195
- Davydov V, Krainer K, Chernykh V (2013) Fusulinid biostratigraphy of the lower Permian Zweikofel formation (Rattendorf Group; Carnic Alps, Austria) and lower Permian Tethyan chronostratigraphy. *Geol J* 48(1):57–100. <https://doi.org/10.1002/gj.2433>
- Eyles N (1993) Earth's glacial records and its tectonic setting. *Earth-Sci Rev* 35:1–248. [https://doi.org/10.1016/0012-8252\(93\)90002-0](https://doi.org/10.1016/0012-8252(93)90002-0)
- Falcon-Lang HJ, Lucas SG, Kerp H, Krainer K, Montañez IP, Vachard D, Chaney DS, Elrick SD, Contreras DL, Kurzawe F, DiMichele WA (2015) Early Permian (Asselian) vegetation from a seasonally

- dry coast in western equatorial Pangea: Paleocology and evolutionary significance. *Palaeogeog Palaeoclimatol, Palaeoecol* 433:158–173. <https://doi.org/10.1016/j.palaeo.2015.05.010>
- Fallgatter C, Paim PSG (2017) On the origin of the Itararé group basal nonconformity and its implications for the late Paleozoic glaciation in the Paraná Basin, Brazil. *Palaeogeogr, Palaeoclimatol Palaeoecol*. <https://doi.org/10.1016/j.palaeo.2017.02.039>
- Fang Q, Wu H, Hinnov LA, Tian W, Wang X, Yang T, Li H, Zhang S (2018) Abiotic and biotic responses to Milankovitch-forced megamonsoon and glacial cycles recorded in South China at the end of the Late Paleozoic Ice Age. *Global and Planetary Change* 163:97–108. <https://doi.org/10.1016/j.gloplacha.2018.01.022>
- Fielding CR, Frank TD, Isbell JL (2008) The late Paleozoic ice age—a review of current understanding and synthesis of global climate patterns. In: Fielding CR, Frank TD, Isbell JL (eds) *Resolving the late Paleozoic ice age in time and space*. Geological Society of America Special, Washington, pp 343–354. [https://doi.org/10.1130/2008.2441\(24\)](https://doi.org/10.1130/2008.2441(24))
- Flügel E (2004) *Microfacies of carbonate rocks. Analysis, interpretation and application*, 2nd edn. Springer, Berlin. <https://doi.org/10.1007/978-3-662-08726-8>
- Forke HC (1995) Biostratigraphie (Fusuliniden; Conodonten) und Mikrofazies im Unterperm (Sakmar) der Karnischen Alpen (Naßfeldgebiet, Österreich). *Jahrb Geol Bundesanst* 138:207–297
- Forke HC (2002) Biostratigraphic subdivision and correlation of uppermost Carboniferous/Lower Permian sediments in the Southern Alps: Fusulinoidean and conodont faunas from the Carnic Alps (Austria/Italy), Karavanke Mountains (Slovenia), and Southern Urals (Russia). *Facies* 47:201–275
- Forke HC, Kahler F, Krainer K (1998) Sedimentology, microfacies and stratigraphic distribution of foraminifers of the lower “Pseudoschwagerina” limestone (Rattendorf Group, Late Carboniferous), Carnic Alps (Austria/Italy). *Senckenb Lethaea* 78:1–39
- Franke W (1989) Tectonostratigraphic units in the Variscan belt of central Europe. In: Dallmeyer RD (ed) *Terranes in the Circum-Atlantic Paleozoic orogens*. Geological Society of America, Washington, pp 67–90
- Gao LF, Ding H, Wan XQ (2005) Taxonomic revision of conodont *Sweetognathus* species in the uppermost Taiyuan Formation, Yuhuai Basin and its significance. *Acta Micropalaeontologica Sinica* 22(4):370–382
- Groves JR, Boardman DR (1999) Calcareous smaller foraminifers from the Lower Permian Council Grove Group near Hooster, Kansas. *J Foraminifer Res* 29(3):243–262
- Groves JR, Wahlman GP (1997) Biostratigraphy and evolution of Late Carboniferous and Early Permian smaller foraminifers from the Barents Sea (offshore Arctic Norway). *J Paleontol* 71:758–779
- Gulbranson EL, Montañez IP, Schmitz MD, Limarino JL, Isbell JL, Marensi SA, Crowley JL (2010) High precision U-Pb calibration of carboniferous glaciation and climate history, Paganzo Group, NW Argentina. *Geol Soc America* 122:1480–1498. <https://doi.org/10.1130/B30025.1>
- Henderson CM (2018) Permian conodont biostratigraphy. *Geol Soc Lond, Special Publ* 450(1):119–142. <https://doi.org/10.1144/SP450.9>
- Henderson CM, Shen SZ (2020) The Permian period. In: Gradstein FM et al (eds) *The geologic time scale*. Elsevier, Netherlands, pp 875–902
- Hua-Zhang P, Erwin DH (2002) Gastropods from the Permian of Guangxi and Yunnan provinces, south China. *J Paleontol* 76:1–49
- Isbell JL, Miller MF, Wolfe KL, Lenaker PA (2003) Timing of Late Paleozoic glaciation in Gondwana: was glaciation responsible for the development of Northern Hemisphere cyclothem? *Geol Soc America* 370:5–24
- Isbell JL, Henry LC, Gulbranson EL, Limarino CO, Fraiser ML, Koch ZJ, Ciccioli PL, Dineen AA (2012) Glacial paradoxes during the late Paleozoic ice age: evaluating the equilibrium line altitude as a control on glaciation. *Gondwana Res* 22:1–19. <https://doi.org/10.1016/j.gr.2011.11.005>
- James NP (1997) *Cool-water carbonates*. SEPM, Tulsa, Oklahoma, USA. <https://doi.org/10.2110/pec.97.56>
- Joachimski MM, von Bitter PH, Buggisch W (2006) Constraints on Pennsylvanian glacioeustatic sea-level changes using oxygen isotopes of conodont apatite. *Geology* 34(4):277–G22198AR. <https://doi.org/10.1130/G22198.1>
- Kahler F, Krainer K (1993) The Schulkofel section in the Carnic Alps, Austria: implications for the Carboniferous-Permian boundary. *Facies* 28(1):257–276
- Kozur HW, LeMone DV (1995) The Shalem Colony section of the Abo and upper Hueco members of the Hueco formation of the Robledo Mountains, Dona Ana County, New Mexico: Stratigraphy and new conodont-based age determinations. *Early Permian Footpr Facies* 6:39–55
- Krainer K, Davydov V (1998) Facies and biostratigraphy of the late Carboniferous/early Permian sedimentary sequence in the Carnic Alps (Austria/Italy). *Geodiversitas* 20(4):643–662
- Krainer K, Flügel E, Vachard D, Joachimski MM (2003) A close look at late Carboniferous algal mounds: Schulkofel, Carnic Alps, Austria. *Facies* 49(1):325–350
- Krainer K, Sanders D, Schaffhauser M (2009) Early Permian shelf margin retreat and carbonate deposition, Zweikofel Massif, Carnic Alps (Austria). *Austrian J Earth Sci* 102(2):134–148
- Krainer K, Lucas SG, Vachard D, Barrick JE, DiMichele WA (2015) The Pennsylvanian-Permian section at Robledo Mountain, Doña Ana County, New Mexico, USA. In: Lucas SG, DiMichelle WA (eds) *Carboniferous-Permian Transition in the Robledo Mountains, Southern New Mexico*. New Mexico Museum of Natural History and Science, Albuquerque, pp 9–41
- Krainer K, Vachard D, Schaffhauser M (2019) Yakhtashian (Artinskian-Early Kungurian) cyanobacteria and calcareous algae from the Carnic Alps (Austria/Italy). *Palaeontol Electron* 22(3):1–107. <https://doi.org/10.26879/931>
- Limarino CO, Césari SN, Spalletti LA, Taboada AC, Isbell JL, Geuna S, Gulbranson EL (2014) A paleoclimatic review of southern South America during the late Paleozoic: a record from icehouse to extreme greenhouse conditions. *Gondwana Res* 25:1396–1421. <https://doi.org/10.1016/j.gr.2012.12.022>
- López-Gamundí OR, Buatois LA (2010) Late Paleozoic glacial events and postglacial transgressions in Gondwana. *Geological Society of America, Boulder, Colorado*. [https://doi.org/10.1130/2010.2468\(00\)](https://doi.org/10.1130/2010.2468(00))
- Läufer A, Hubich D, Loeschke J (2001) Variscan geodynamic evolution of the Carnic Alps (Austria/Italy). *Int J Earth Sci* 90(4):855–870
- Lucas SG, Krainer K, Vachard D (2015) The Lower Permian Hueco Group, Robledo Mountains, New Mexico (USA). In: Lucas SG, DiMichelle WA (eds) *Carboniferous-Permian Transition in the Robledo Mountains, Southern New Mexico*. New Mexico Museum of Natural History and Science Bulletin, Albuquerque, pp 43–95
- Manifold L, Hollis C, Burgess P (2020) The Anatomy of a Mississippian (Viséan) carbonate platform interior, UK: depositional cycles, glacioeustasy and facies mosaics. *Sed Geol*. <https://doi.org/10.1016/j.sedgeo.2020.105633>
- Manifold L, del Strother P, Gold DP, Burgess P, Hollis C (2021) Unravelling evidence for global climate change in Mississippian carbonate strata from the Derbyshire and North Wales Platforms, UK. *J Geol Soc*. <https://doi.org/10.1144/jgs2020-106>
- Mory AJ, Redfern J, Martin JR (2008) A review of Permian-Carboniferous glacial deposits in western Australia. In: Fielding CR, Frank TD, Isbell JL (eds) *Resolving the Late Paleozoic Ice Age in Time and Space*. Geological Society of America Special Paper, 441:29–40

- Pinard S, Mamet B (1998) Taxonomie des petits Foraminifères du Carbonifère Supérieur–Permien Inférieur du Bassin de Sverdrup, Arctique Canadien. Geological Association of Canada, St. Johns, Newfoundland
- Read MT, Nestell MK (2018) Cisuralian (Early Permian) Sweetognathid conodonts from the upper part of the Riepe Spring Limestone, north Spruce Mountain ridge, Elko County, Nevada. In: Over DJ, Henderson CM (eds) Conodont Studies dedicated to the careers and contributions of Anita Harris, Glenn Merrill, Carl Rexroad, Walter Sweet and Bruce Wardlaw, *Bulletins of American Paleontology*, 395–396:89–113
- Read MT, Nestell MK (2019) Lithostratigraphy and fusulinid biostratigraphy of the Upper Pennsylvanian–Lower Permian Riepe Spring Limestone at Spruce Mountain Ridge, Elko County, Nevada, USA. *Stratigraphy* 16(4):195–247. <https://doi.org/10.29041/strat.16.4.195-247>
- Ritter SM (1986) Taxonomic revision and phylogeny of post-Early Permian crisis *bisselli-whitei* Zone conodonts with comments on late Paleozoic diversity. *Geol Palaeontol* 20:139–165
- Rygel MC, Fielding CR, Frank TD, Birgenheier LP (2008) The magnitude of Late Paleozoic glacioeustatic fluctuations: a synthesis. *J Sediment Res* 78(8):500–511
- Samankassou E (1999) Drowning of algal mounds: records from the Upper Carboniferous lower *Pseudoschwagerina* Limestone, Carnic Alps, Austria *Sedimentary Geology* 127(3–4):209–220. [https://doi.org/10.1016/S0037-0738\(99\)00052-4](https://doi.org/10.1016/S0037-0738(99)00052-4)
- Schaffhauser M (2013) The Trogkofel Formation: Sedimentology and diagenesis of a rimmed carbonate shelf margin in the Lower Permian of the Carnic Alps (Austria/Italy). Dissertation, University of Innsbruck
- Schaffhauser M, Krainer K, Sanders D (2010) The Zottachkopf Formation: a new formation in the Lower Permian Rattendorf Group (Carnic Alps, Austria). *J Alpine Geol* 52:218–219
- Saltzman MR, González LA, Lohmann KC (2000) Earliest Carboniferous cooling step triggered by the Antler orogeny? *Geology* 28(4):347–350
- Stemmerik L (2008) Influence of late Paleozoic Gondwana glaciations on the depositional evolution of the northern Pangean shelf, North Greenland, Svalbard, and the Barents Sea. *Resolving the late Paleozoic ice age in time and space* 441:205–217
- Vesely FF, Trzaskos B, Kipper F, Assine ML, Souza PA (2015) Sedimentary record of a fluctuating ice margin from the Pennsylvanian of western Gondwana: Paraná Basin, southern Brazil. *Sed Geol* 326:45–63. <https://doi.org/10.1016/j.sedgeo.2015.06.012>
- Wahlman GP (2019) Pennsylvanian and Lower Permian fusulinid biostratigraphy of the Permian Basin region, southwestern USA. In Ruppel SC (ed) *Anatomy of a Paleozoic basin: the Permian Basin USA* (vol.1, ch.7). The University of Texas at Austin, Bureau of Economic Geology report of investigations 285. American Association of Petroleum Geologists Bulletin 118:167–227
- Springer Nature or its licensor (e.g. a society or other partner) holds exclusive rights to this article under a publishing agreement with the author(s) or other rightsholder(s); author self-archiving of the accepted manuscript version of this article is solely governed by the terms of such publishing agreement and applicable law.